A curative combination therapy for lymphomas achieves high fractional cell killing through low cross-resistance and drug additivity but not synergy

Adam C Palmer[1*], Christopher Chidley[1*], and Peter K Sorger[1,2]

[1] Laboratory of Systems Pharmacology
[2] Department of Systems Biology
Harvard Medical School
200 Longwood Avenue
Boston MA 02115

*These authors contributed equally.

† Pre-publication correspondence should be addressed to Peter Sorger (peter_sorger@hms.harvard.edu); copying Chris Bird (617-432-6901/6902).

Peter K Sorger: orcid.org/0000-0002-3364-1838

SUMMARY

Curative cancer therapies are uncommon and nearly always involve multi-drug combinations developed by experimentation in humans; unfortunately, the mechanistic basis for the success of such combinations has rarely been investigated in detail, obscuring lessons learned. Here we use isobologram analysis to score pharmacological interaction, and clone tracing and CRISPR screening to measure cross-resistance among the five drugs comprising R-CHOP, a combination therapy that frequently cures Diffuse Large B-Cell Lymphomas. We find that drugs in R-CHOP exhibit very low cross-resistance but not synergistic interaction; together they achieve a greater fractional kill according to the null hypothesis for both the Loewe dose-additivity model and the Bliss effect-independence model. These data provide direct evidence for the 50-year old hypothesis that a curative cancer therapy can be constructed on the basis of independently effective drugs having non-overlapping mechanisms of resistance, without synergistic interaction, which has immediate significance for the design of new drug combinations.

INTRODUCTION

The majority of cancers are treated with combination therapies. For some types of cancer, multidrug combinations produce frequent cures, whereas cure by monotherapy is rare (Frei and Antman, 2000). In current practice, the search for new drug combinations focuses on identifying drugs that exhibit synergy. Although "synergy" is often used loosely it is best defined by Bliss or Loewe criteria, which test whether a combination is stronger than expected from the sum of the drugs' individual effects; antagonism arises when combinations are less active than additivity would predict. In translational cancer biology such measurements are most commonly made using cultured cells or genetically defined mouse models. Despite the current emphasis on synergy, historically successful combinations were developed according to quite different hypotheses. For example, Law and Frei et al. argued for combining drugs that are independently effective and have non-overlapping mechanisms of resistance(Frei et al., 1965; Law, 1956, 1952). Such combinations are expected to overcome clonal heterogeneity present within each patient's cancer. Heterogeneity between patients can also be a reason why drug combinations improve response rates, even when each patient only benefits from the most active monotherapy. However, cure is almost never achievable by monotherapy, and the superiority of curative combinations cannot be explained by patient variability in best single-drug response (the topic of our previous work (Palmer and Sorger, 2017)).

The pharmacological principles underlying curative combination therapies are largely unknown because they were generally developed via empirical experimentation in patients, and have only rarely been subjected to detailed mechanistic analysis. Knowing the design principles behind these existing curative regimens would assist in rationally assembling new cancer medicines into potentially curative combinations. A key question in contemporary drug discovery is determining which among several different properties of a combination should be given the greatest weight: strong individual activity and

low cross-resistance as proposed five decades ago, or synergistic interaction as currently emphasized (e.g. (Han et al., 2017; Rationalizing combination therapies, 2017)).

Testing whether a higher order multi-drug combination exhibits synergistic interaction can only be accomplished *ex vivo* by measuring and analyzing the responses of cells to drugs applied individually and in combination over a range of concentrations, for example by isobologram analysis (Greco et al., 1995; Loewe, 1953). When evaluated at fixed doses the superiority *in vivo* of a combination over monotherapy can occur without a true pharmacological interaction and is therefore not sufficient evidence of synergy (Berenbaum, 1989). Testing whether a combination exhibits low cross-resistance is more challenging because it requires systematic exploration of resistance mechanisms; different mechanisms of resistance display different cross-resistance properties. It has long been possible to isolate cell clones resistant to single drugs and then assay for sensitivity to other drugs, but this approach is not practical at a scale needed to test Law and Frei's hypothesis, as was recognized by Law himself (1956). Efficient analysis of cross-resistance has become feasible only recently with technical breakthroughs in multiplexed clone tracing and reverse genetic screening. DNA barcode libraries allow large numbers ($\geq 10^6$) of uniquely tagged clones to be tested in parallel for resistance to multiple drugs (Bhang et al., 2015), and genetic screens using CRISPR-Cas9 technologies enable genome-wide identification of loss and gain of function changes that confer resistance (Bhang et al., 2015; Gilbert et al., 2014; Jost et al., 2017; Shalem et al., 2014; Wang et al., 2014). To date, barcode and CRISPR-Cas9 libraries have been used to study mechanisms of resistance primarily to targeted therapies and identify new combinations of such drugs (Bhang et al., 2015; Hata et al., 2016); they have not yet been used to test Law and Frei's 'non-overlapping resistance' hypothesis by analyzing combinations of cytotoxic drugs that are the backbone of curative therapies.

In this paper we measure pharmacological interaction and cross-resistance among components of R-CHOP, a five drug chemo-immunotherapy that achieves high cure rates in Diffuse Large B-Cell

Lymphoma (DLBCL). R-CHOP has five constituents: R – rituximab, a humanized monoclonal antibody against CD20, a protein expressed on the surface of all B cells; C – cyclophosphamide (Cytoxan®) an alkylating agent; H – hydroxydaunomycin (doxorubicin, or Adriamycin®), a topoisomerase II inhibitor; O – Oncovin® (vincristine), an anti-microtubule drug and; P – prednisone, a steroid. R-CHOP was developed over an extended period of time via clinical experiments in humans (Lakhtakia and Burney, 2015). The constituents of R-CHOP are known to be individually cytotoxic to DLBCL cells *in vivo*, and the drugs have largely non-overlapping dose-limiting toxicities, which permits their combined administration in patients. The reasons for the clinical superiority of R-CHOP in DLBCL remain poorly understood. Pritchard et al. (2013) observed no synergy among pairs of drugs in CVAD (similar to CHOP) in a mouse cell line model of Non-Hodgkin lymphoma, and in profiling the effects of 93 gene knockdowns by RNA interference on drug sensitivity, the change in sensitivity to CVAD was equal (for almost every knockdown) to the average of its changes in single-drug sensitivity; this demonstrates that CVAD does not act as a more potent version of a single drug, nor does it exhibit a new signature of genetic dependencies.

We tested for pharmacological interaction among all pairs of R-CHOP constituents across a full dose range in three DLBCL cell lines and assessed interaction using both the Bliss independence and Loewe additivity criteria. We observed little if any synergy: most drug pairs were additive and some were antagonistic. We also tested higher order combinations at fixed dose ratios with similar results. We then screened for cross resistant mutations using random mutagenesis with clone tracing as well as CRISPR interference (CRISPRi) and CRISPR activation (CRISPRa) with genome-scale libraries. The rate of multi-drug resistance was near the theoretical minimum predicted by Law (1952), where the 'fractional killing' achieved by a combination is the product of each individual drug's fractional kill. This suggests that high single-agent activity and low-cross-resistance are key attributes of the curative R-CHOP regimen.

RESULTS

Components of R-CHOP do not exhibit synergy in killing Diffuse Large B-Cell Lymphoma cells

Pharmacological interactions among R-CHOP constituents were measured in human Pfeiffer, SU-DHL-4 and SU-DHL-6 cell lines. All three lines are derived from germinal center B-like DLBCL, the subtype most responsive to R-CHOP (Alizadeh et al., 2000). Prednisone and cyclophosphamide are pro-drugs that are activated by liver metabolism. We therefore used the pre-activated forms of these drugs: prednisolone and 4-hydroperoxy-cyclophosphamide (which spontaneously converts to the active compound 4-hydroxy-cyclophosphamide in water) (Ludeman, 1999). Rituximab kills B-cell lymphomas through multiple CD20-dependent mechanisms that include complement-mediated cytotoxicity (CMC), antibody-dependent cell cytotoxicity (ADCC) and direct killing via CD20 cross-linking (Weiner, 2010). Consistent with previous reports (Kobayashi et al., 2013), we observed that Rituximab can kill DLBCL cells in culture via CMC when human serum is included in the culture media (Figure S1A). Among seven DLBCL cell lines tested, none exhibited a cytotoxic response to prednisolone alone at clinically relevant concentrations, although the rate of cell division was reduced (Figure S1B). Prednisone is cytotoxic to DLBCL in first-line clinical care (Lamar, 2016); the absence of cytotoxicity in DLBCL cell culture, consistent with other studies (Knutson et al., 2014), might reflect selection for complete prednisone resistance in cell lines established from post-treatment patients. As there exist no generally available treatment-naïve DLBCL cell lines, we are not able to test whether such cultures might respond *in vitro* to prednisolone.

Pharmacodynamic interactions among drugs comprising R-CHOP were first measured in Pfeiffer cells. For each of 10 drug pairs an 11×11 ‘checkerboard’ was created with each drug increasing in concentration along one of the two axes, spanning a 100-fold range. Cells were incubated with drugs for 72 hours, which spans at least one *in vivo* half-life in humans for each of C, H, O and P (de Jonge et al.,

2005; Gidding et al., 1999; Speth et al., 1988); R has an elimination half-life of 3 weeks in humans (Tran et al., 2010). Cell viability was measured using a luminescent ATP assay (CellTiter-Glo) that was linearly proportional to live cell number as determined by microscopy and vital stain (Figure S1C). The ratio of cell number in drug-treated and untreated control cultures (relative cell number) was used to compute normalized growth rate inhibition values (GR values (Hafner et al., 2016)) (Figure S1D). Pharmacological interaction was then assessed based on excess over Bliss Independence and by isobologram analysis (which tests for Loewe additivity (Berenbaum, 1989)). We have previously used isobologram analysis to confirm synergistic interaction among HER2 and CDK4/6 inhibitors in breast cancers, which serves as a positive control for the identification of synergy by drug-drug 'checkerboard' experiments (Goel et al., 2016).

In the Bliss model, drugs are scored as interacting only if their combined effect exceeds a null model of independence involving statistically independent probabilities of cell killing (Bliss, 1939). By this analysis, we find that pairs of drugs in R-CHOP are largely independent, except that killing by O is strongly antagonized by the presence of either C or H (Figure 1A). Antagonism may be a consequence of the effects of these drugs on the cell cycle: killing of mitotic cells by O is expected to decrease when C- or H-induced DNA damage prevents entry into mitosis (Barlogie et al., 1976; Cutts, 1961; Davidoff and Mendelow, 1993).

In isobologram analysis, contour lines (isoboles) corresponding to a constant phenotype (the fraction of cells killed) are plotted across a two-way dose-response landscape (Greco et al., 1995; Loewe, 1953). The shape of the contours is diagnostic of drug interaction: straight contours correspond to drug additivity, convex contours to synergy and concave contours to antagonism (Figure 1B, inset). Isobologram analysis of drug pairs in R-CHOP confirmed results from Bliss analysis, namely that interactions among R-CHOP constituents range from strongly antagonistic to approximately additive (Figure 1B). As discussed earlier, prednisolone was not cytotoxic on its own but it slightly sensitized

cells to C and to H. Moreover, CMC by rituximab was approximately additive with each of C, H, and O. As was observed using the Bliss method of analyzing drug interaction, C and H severely antagonized O. Overall, no drug pair showed a beneficial effect exceeding 2-fold deviation from additivity, the minimal recommended threshold for avoiding false-positive claims of synergy (Odds, 2003).

To test for higher order interactions, we exposed each of the three different DLBCL cell lines to all 26 possible combinations of 2, 3, 4, or 5 drugs (Figure 2A). Because high-order combinations cannot feasibly be studied across multi-dimensional dose 'checkerboards', R-CHOP constituents were tested at fixed ratios scaled so that constituents were equipotent with respect to cell killing when assayed individually (Figure S2A). The activity of drug combinations was then quantified by *Fractional Inhibitory Concentrations* (FIC (Elion et al., 1954), also known as *Combination Index* (Chou, 2010)), which is a fixed-ratio simplification of Loewe's isobologram analysis (additive contours have FIC=1 by definition). In all three DLBCL cultures, we observed that small excesses over additivity for R and P on CHO was balanced by antagonism within CHO, producing net effects ranging from approximately additive to antagonistic (for 5-drugs in Pfeiffer FIC = 0.80±0.15; for SU-DHL-6 FIC = 1.1±0.3 and for SU-DHL-4 FIC = 1.7±0.2; 95% confidence, n=4-8; Figures 2B and 2C). The absence of synergy across high-order combinations was supported by Bliss analysis of the same data (Figure S2B). Emergent pharmacological interactions involving combinations of 3 or more drugs can be identified as deviations from the assumption of dose additivity using data from lower order drug interactions (Cokol et al., 2017); nearly all such terms supported the hypothesis of no interaction (emergent FIC=1) with the only substantial deviations representing mild antagonism (emergent FIC up to 1.5) (Figure S2C). We conclude that R-CHOP does not exhibit significant synergy among its constituent drugs in cell culture.

DLBCL clones resistant to one drug in R-CHOP rarely resist multiple drugs

To test the hypothesis that low cross-resistance is important for a curative therapy we asked whether clones resistant to any single drug in R-CHOP remain susceptible to at least one other drug in the combination. DLBCL genomes are relatively complex, possessing a mixture of single nucleotide polymorphisms and copy number gains and losses (Pasqualucci et al., 2011; Sebastian et al., 2016), and we therefore looked for resistance mutations using three complementary approaches: (i) random mutagenesis coupled to clone tracing, (ii) genetic knockdown via CRISPR interference (CRISPRi) for loss of function mutations, and (iii) overexpression via CRISPR activation (CRISPRa) for gain of function mutations (Figure 3A). In a hypothetical multi-drug treatment, it is not possible to distinguish between single-drug or multi-drug resistance as either could increase the survival of a mutated clone (Figure 3B). A further complication is that strongly antagonistic drug combinations, such as C, H, and O, can select for *sensitivity* to the antagonizing agent (Chait et al., 2007). We therefore scored mutations as conferring true cross-resistance by applying drugs individually and identifying mutant cells that were significantly enriched in two or more conditions (Figure 3C). This was accomplished by generating a pool of mutagenized/CRISPR-transformed cells in which each cell carried a unique DNA barcode (or single guide RNA (sgRNA) that also acts as a barcode). Cells were split into independent cultures and then treated with a single R-CHOP component. The abundance of DNA barcodes in each culture was measured before and after drug exposure by high-throughput DNA sequencing followed by enrichment analysis.

For random mutagenesis and clone tracing, Pfeiffer cells were mutagenized with N-ethyl-N-nitrosourea (ENU), which induces point mutations and chromosome aberrations (Sanger and Eisen, 1976; Shibuya and Morimoto, 1993). One million mutagenized clones were barcoded using a lentiviral DNA barcode library (ClonTracer; (Bhang et al., 2015)). Due to high library complexity ($\approx 7\times10^7$ barcodes) and infection at low multiplicity (0.1), over 99% of clones are expected to contain a unique barcode. Barcoded cells were expanded in puromycin to select for the lentiviral vector. From a single

well-mixed suspension of cells, a batch was reserved to measure pre-treatment barcode frequencies, and the remainder was distributed into 18 replicate cultures (3 per drug tested) with each culture providing 12-fold coverage of barcoded clones (Figure S3A).

To model the clinical scenario of strong selection pressure from intensive treatment cycles (as opposed to continuous low dose therapy), drugs were applied for 72 hours at a dose established in a pilot study as the highest dose allowing any surviving cells to re-grow in drug-free media in under 2 weeks (Methods). Cultures were exposed to two rounds of drug treatment followed by a recovery period of 4 to 11 days as needed (Figure S3A). Because prednisolone monotherapy only slowed growth, which is difficult to score in a short duration culture, cells were treated with prednisolone at 20 μM for 20 days (the R-CHOP regimen contains multiple five-day courses of prednisone). Enrichment for specific clones was calculated based on relative barcode frequencies prior to and after treatment.

Thousands of clones were reproducibly enriched in replicate cultures exposed to the same drug. To score cross-resistance and account for culture-to-culture variation across repeats, we constructed an error model by scrambling barcode identities within each replicate. This revealed that at least 300 times as many barcodes were ≥10-fold enriched in repeat experiments for any single drug than expected by chance (Figure 4A). We also accounted for fitness differences observed in vehicle-only cultures (~1% of barcodes were enriched ≥ 10-fold in the presence of DMSO; see Methods). Correlations between enrichment scores in replicate drug treatments were highly significant ($p<10^{-900}$; $n\approx 10^{6}$) although of modest magnitude (0.1 to 0.3) (Figure 4B). This arises because drug exposure imposes population bottlenecks on non-resistant clones, which represent the majority of the population, causing barcodes to be detected, or not, on a stochastic basis. Among barcodes with non-zero counts in replicate experiments, correlation was higher (0.35 to 0.58). We used the geometric mean of enrichment for each barcode as a metric of drug resistance across replicates. Instances of stochastic (and thus irreproducible)

enrichment are strongly penalized by this metric; conversely, barcodes are favored if they are reproducibly enriched in independent cultures (which is evidence of heritability).

The error model constructed from scrambled barcodes was used to estimate the false discovery rate for barcode enrichment. We found that the stronger the geometric mean enrichment, the less likely it was for enrichment to occur randomly (Figure 4C). False discovery of coincident enrichment exceeding 10-fold in two or more drugs was rare (<2.5%) and we therefore selected this threshold for subsequent analysis. For each of the four individually active drugs (i.e. RCHO), 2,000 to 13,000 barcodes were identified with geometric mean enrichment ≥10-fold, representing resistance frequencies of 2×10^{-3} to 1×10^{-2}. The vast majority of enriched clones were unique to one drug, with only 30 to 300 clones (depending on the pair of drugs) enriched in two different conditions; the latter is diagnostic of double-drug resistance (Figures 4D and 4E). Triple-drug resistant clones were even less abundant (between 1 and 10 clones per set of three drugs) and no clones were identified that conferred resistance to R, C, H and O (Figure 4E). Clones enriched by prolonged exposure to prednisolone at concentrations that slowed growth also exhibited low overlap with barcodes enriched for other constituents of R-CHOP (Figures S4A and S4B).

CRISPRi/a screening identifies diverse mechanisms of drug resistance

Screening genome-wide sgRNA libraries using CRISPR-Cas9 has the advantage that it yields the identities of genes conferring drug resistance as opposed to barcodes for unknown ENU-mutated loci. CRISPRi screening identifies loss of function resistance mutations and was performed in Pfeiffer cells by expressing nuclease-dead Cas9 fused to the transcriptional repression domain KRAB (dCas9-KRAB) (Gilbert et al., 2013). CRISPRa screening identifies overexpression resistance mutations and was performed in cells by co-expressing dCas9 fused to SunTag (a repeating peptide array) and a SunTag-binding antibody fused to the VP64 transcriptional activator (Tanenbaum et al., 2014). This

approach requires clonal selection of a co-expressing cell line in which the ratio of dCas9:VP64 is fixed; otherwise, cell-to-cell variability complicates screening for overexpression phenotypes. However, we were unable to generate monoclonal lineages of Pfeiffer cells expressing dCas9 and VP64. In other DLBCL cell lines, lentiviral transduction was inefficient (a known property of B lymphocytes and lymphomas (Li et al., 2001)). We therefore performed CRISPRa screens in the chronic myeloid leukemia (CML) cell line K562, which can be efficiently transduced and cloned. For CRISPRi in Pfeiffer cells it was possible to screen for resistance to four drugs (R, C, H and O) but for CRISPRa in K562 cells, screening was possible only for C, H and O. Of note, these drugs have been used historically in the treatment of CML, and we validated (below) that screen hits identified in K562 could be reproduced in DLBCL.

We used RT-qPCR to confirm that transduction of sgRNAs in cells expressing the appropriate dCas9 fusion protein caused strong repression of a set of test target genes by CRISPRi and strong activation by CRISPRa (Figure S5A). We then used lentivirus at low multiplicity ($\leq$0.4) to infect CRISPRi and CRISPRa-expressing cells with second generation genome-scale sgRNA libraries, which are highly active by virtue of having optimized target sites that account for nucleosome positioning (Horlbeck et al., 2016). Both libraries contain 10 sgRNAs per gene, and approximately 4,000 control sgRNAs designed to have no target. Following expansion, infected cells were exposed to drug (or vehicle) for two to three 72-hr drug pulses separated by recovery periods of up to 5 days as needed (Figures S3B and S3C). Sequencing of sgRNAs was then used to identify hits (Tables S4 and S5). The impact of each sgRNA on drug sensitivity was quantified by the 'rho phenotype' (Kampmann et al., 2013), which is 1 in the case of complete resistance, 0 in the case of sensitivity matching the parental cell line (as determined using non-targeting control sgRNAs), and <0 for hypersensitivity (Methods; Tables S6 and S7). Across 10 sgRNAs for each gene we calculated the mean of the strongest 5 rho phenotypes by absolute value, and the p-value of all 10 rho phenotypes as compared to the 4,000 control

sgRNAs (Mann-Whitney test) (Gilbert et al., 2013). Random permutations of 10 control sgRNAs were assembled to create ≈19,000 'negative control genes', matching the number of real gene targets and with phenotypes specific to each drug screen. For all drugs tested, plots of gene phenotype vs. significance ('volcano plots') revealed many gene perturbations conferring drug resistance or hypersensitivity (Figure 5, and Tables S8 and S9).

Hits from CRISPRi and CRISPRa were consistent with known mechanisms of drug action: knockdown of direct targets was observed to confer resistance to rituximab (*MS4A1* encoding CD20) and doxorubicin (*TOP2A* encoding topoisomerase II) (Thorn et al., 2011; Weiner, 2010) whereas overexpression of *TUBB* (which encodes β-tubulin) conferred resistance to vincristine. Cyclophosphamide functions by inducing interstrand crosslinks in genomic DNA via alkylation. CRISPRi identified multiple genes involved in the DNA damage response: cyclophosphamide resistance was conferred, for example, by knockdown of *SLFN11* which blocks progression of stressed replication forks (Murai et al., 2018; Zoppoli et al., 2012) and hypersensitivity (measured in a supplemental screen at a lower cyclophosphamide dose; Figures S5B and S5C) was caused by knockdown of genes involved in DNA interstrand crosslink repair (e.g. *FANCE*, *FANCD2*, *UBE2T*, *FANCI*, *ATRIP*) and double-strand break repair (e.g. *BRIP1*, *BARD1*, *BRCA1*, *BRCA2*). The therapeutic window for cyclophosphamide arises from tissue-specific expression of aldehyde dehydrogenases (ALDHs) which are the primary enzymes involved in cyclophosphamide inactivation (Cox et al., 1975); overexpression of *ALDH1A1* and *ALDH1B1* as well as aldo-keto reductases (AKRs) that metabolize cytotoxic products of cyclophosphamide (Penning, 2017) all conferred resistance in our screen. Detailed study of these genes is beyond the scope of this manuscript (full results are in Tables S8 and S9) but from these data we conclude that CRISPRi/a screening successfully identifies biologically relevant genes involved in resistance to RCHO.

To test the robustness of results from whole-genome screens, we performed individual validation studies with selected sgRNAs. We constructed single knockdown or overexpression cell lines for each of nine CRISPRi and eight CRISPRa sgRNAs conferring single or multi-drug resistance phenotypes, and measured their drug sensitivity in dose-response experiments (for a total of 9 genes × 4 drugs = 36 validation experiments for CRISPRi; 8 × 3=24 for CRISPRa). The IC_{50} values for drug responses in Pfeiffer cells as measured in CRISPRi validation experiments were strongly correlated with resistance phenotypes from the original knockdown screen (r = 0.66, $P < 10^{-5}$; n=36 gene-drug interactions; Figures 6A and S6A) as were IC_{50} values for CRISPRa validation studies in K562 CML cells (r = 0.84, $P < 10^{-5}$; Figure 6B and S6B). To test if resistance genes identified in K562 cells have similar phenotypes in DLBCL cells, we generated a polyclonal CRISPRa Pfeiffer cell culture and derived individual overexpression mutants by transduction of single sgRNAs. Gene overexpression is less efficient in this setting than in K562 cells (Figure S6B) but we nonetheless found that CRISPRa produced changes in IC_{50} values in Pfeiffer cells that were strongly correlated with changes observed in K562 validation experiments (r = 0.82, $P < 10^{-5}$; n=24 gene-drug interactions) and with resistance phenotypes obtained in the overexpression screen in K562 (r = 0.62, $P = 0.001$; Figures S6C and S6D).

To measure overexpression-mediated drug resistance with greater sensitivity, we also performed competition assays by mixing two Pfeiffer cultures, one expressing a gene-targeting sgRNA from the validation studies described above and the second a non-targeting sgRNA. We then measured the change in the ratio of cultures by qPCR following two cycles of drug treatment and recovery (in the same manner as for genome-wide screens; Figure S3). These experiments demonstrated a strong correlation between sgRNA-induced competitive fitness in DLBCL cells grown in the presence of drug and drug resistance as measured in the overexpression screens (r = 0.69, $P = 0.0002$; Figure 6C). We conclude that genome-wide knockdown and overexpression screens yielded robust and reproducible

hits, and that overexpression-mediated resistance identified in K562 cells is largely recapitulated in DLBCL cells.

Knockdown and overexpression mutations identified by CRISPRi/a do not confer pan-drug resistance

Next we asked whether any of the gene perturbations identified by knockdown or overexpression screening conferred resistance to multiple drugs. For each screen, we calculated a single resistance score that takes into account both effect size and the significance of enrichment (mean rho phenotype $\times$ -$\log_{10}$P). We selected a cut-off in resistance scores that yielded less than one false-positive example of multi-drug resistance per ≈19,000 negative control genes (the number of real gene targets). This cut-off is lenient in scoring for single-drug resistance but by reducing the chance that true cross-resistance will be missed, it ensures a *more* stringent test of Law and Frei's hypothesis (Figures S7A and S7C). CRISPRi yielded 19 genes whose knockdown conferred resistance to two drugs, and 4 genes conferring resistance to three drugs (Figures 7A, 7B and S7B). For example, resistance to rituximab and doxorubicin was conferred by CRISPRi of *SMARCE1*, a known tumor suppressor in DLBCL and other cancers (Shain and Pollack, 2013), and by CRISPRi of *CAD*, a protein involved in pyrimidine biosynthesis whose knockdown causes S phase arrest (Jost et al., 2017). Genes that conferred triple resistance when knocked down were involved in translation initiation, chromatin modification, protein degradation and the mediator complex; these gene knockdowns conferred mild resistance as compared to those producing single and double resistance (resistance score < 2) and also reduced cell proliferation in the absence of drug (p-value for growth defect < 10^{-5}; Table S2). Thus, these multi-drug resistance genes may act by reducing rates of proliferation, a phenotype that generally predisposes cells to chemotherapy resistance (as reported for *CAD*; (Jost et al., 2017)). No genes were identified by CRISPRi whose knockdown conferred resistance to every drug in RCHO.

Screening by CRISPRa identified 42 genes whose overexpression conferred resistance to two drugs and 4 genes that conferred resistance to three drugs (Figures 7C, 7D and S7D). Overexpression of the *ABCB1* and *ABCC1* ATP-binding cassette (ABC) transporters resulted in resistance to H and O, but not to C (Figure 7C), and overexpression of the *ABCG2* ABC transporter conferred resistance to H alone (Figure 5); upregulation of drug export via overexpression of ABC transporters has been implicated in resistance to many drugs (Choi, 2005). Two of four genes whose activation conferred triple-drug resistance (to C, H and O) were linked to glutathione biosynthesis: *GCLC*, which catalyzes the first step in glutathione production, and *NFE2L2*, a transcription factor for *GCLC* and other genes involved in response to xenobiotics and oxidative stress (Figure 7C) (Kitamura and Motohashi, 2018; Zanotto-Filho et al., 2016). Glutathione plays an important role in resistance to chemotherapy (Bansal and Simon, 2018), and high expression of glutathione family genes is strongly associated with poor overall survival in DLBCL on CHOP (Andreadis et al., 2007). Further supporting the importance of glutathione for chemotherapy responsiveness, knockdown of *GCLC* conferred hypersensitivity to H and O, and knockdown of the main transporter of cystine (which is limiting for glutathione synthesis), *SLC7A11*, conferred hypersensitivity to H (Figure 5). Thus, CRISPRa identified multiple genes associated with previously described or suspected mechanisms of drug resistance, but even genes associated with 'multi-drug resistance' such as ABC transporters were observed to confer resistance to only a subset of drugs.

Cross-resistance between drugs in RCHOP is close to a theoretical minimum

The degree to which two drugs are subject to shared or distinct resistance mechanisms is expected to vary depending on the drugs, and can be described by a cross-resistance parameter ξ, where $0 \leq \xi \leq 1$. As Law described in 1952 (Law, 1952) , if one cell in 10^A has resistance to drug *a*, and one cell in 10^B has resistance to drug *b*, then at least one cell in 10^{A+B} will be resistant to both drugs by chance; this theoretical minimum is described by $\xi = 0$. The largest possible frequency of cross-

resistance is the smaller of the single-drug resistance frequencies, a situation described by $\xi = 1$. Any observed frequency of cross-resistance can be quantified as a weighted sum of the minimum and maximum possibilities to give a value of ξ between 0 and 1 (Methods). To estimate ξ in clone-tracing studies on ENU-mutagenized cells, we first performed two independent sets of clone tracing experiments (each in triplicate) for resistance to O alone. Perfect replicates should result in $\xi = 1$; we compared different concentrations of O to mimic differences between drugs in rates of killing, and observed $\xi = 0.69$ (Figures S4C and S4D). Next, examining all combinations of 2, 3 or 4 drugs we observed uniformly low ξ, with an average value of $\xi = 0.016$ (Figures 8A and 8B). This indicates that although we observed substantial co-occurrence of clones across drugs, they do not all represent truly cross-resistant mutations, because their frequency can be largely accounted for by the independent acquisition of multiple mutations that each confer resistance to a single drug. Thus, we observed that randomly mutagenized cells exhibited nearly the theoretical minimum rate of cross-resistance, with an absolute frequency of resistance to all drugs in R-CHOP $<< 10^{-6}$.

In CRISPR screens single gene perturbations are analyzed and only true cross-resistance is detected. Law's prediction can still be applied: if resistance to drugs *a* and *b* is conferred by a fraction of CRISPR perturbations (at frequencies 10^{-A} and 10^{-B}) with $\xi = 0$, perturbations conferring resistance may coincidentally overlap at a frequency of $10^{-(A+B)}$. In CRISPRi and CRISPRa screens, rates of multi-drug resistance exceeded this minimum, largely due to genes such as transporters whose function is protection against multiple xenobiotics. For example in CRISPRa screens, the theoretical minimum number of 2-drug resistant genes is predicted to be 1 ($\xi = 0$) and the maximum number 132 ($\xi = 1$); the observed average for all drug pairs was 18 ($\xi = 0.13$). Considered together, CRISPRi and CRISPRa screens exhibited an average cross-resistance value of ξ=0.05. We therefore conclude that multi-drug resistance to the drugs making up R-CHOP is close to its minimum predicted value.

Other applications: hypersensitivity as a guide to vulnerabilities

The identification of genes involved in drug hypersensitivity has the potential to uncover interactions causing 'collateral sensitivity' and other druggable vulnerabilities. We analyzed drug hypersensitivity in the same manner as resistance (Methods, Figures S8A and S8C) and found that, among 778 CRISPRi or CRISPRa resistance genes, only 13 (1.7%) exhibited hypersensitivity to a different drug. Thus, collateral sensitivity is unlikely to play a major role in R-CHOP therapy, although it may be relevant to other drug combinations. We also identified multiple genes conferring hypersensitivity to two drugs, and three genes conferred hypersensitivity to three drugs (no genes were found that made cells hypersensitive to 4 drugs; Figures S8B and S8D). For example CRISPRa of *LMO2* sensitized cells to C and O; *LMO2* is highly expressed in the Germinal Center subtype of DLBCL, which responds better to R-CHOP than the *LMO2*-low Activated B-Cell subtype (Alizadeh et al., 2000). Across all subtypes, high *LMO2* expression is the strongest single gene predictor of survival in DLBCL patients treated with CHOP or R-CHOP (Lossos et al., 2004; Natkunam et al., 2008). Thus, the prognostic value of *LMO2* may be mediated in part through its impact on sensitivity to cyclophosphamide and vincristine. Hypersensitivity genes may be addressable therapeutically since 11% (23 from by CRISPRi and 49 from CRISPRa) are members of the 'liganded genome' – the subset of proteins for which high affinity small molecules are available (Moret et al., 2019; Roberts et al., 2017). Study of such compounds is beyond the scope of the current study but our data suggest possible avenues to enhancing responsiveness to R-CHOP in DLBCL.

DISCUSSION

The use of cancer drugs in combination was motivated historically by the need to overcome selection for drug resistance, which is a primary limitation on the durability of responses to monotherapy (Law, 1952). Inspired in part by multi-drug cures for tuberculosis, it was proposed that lasting remission

required combined use of chemotherapies having different mechanisms of action and thus, different mechanisms of resistance (see retrospectives by Frei and Antman, 2000; Schnipper, 1986). Recent mathematical models of tumor evolution support these ideas, and predict that curing a cancer requires non-cross-resistant drug combinations in which the probability of acquiring resistance to all drugs is effectively zero (given the number of tumor cells and the magnitude of tumor cell killing) (Bozic et al., 2013). In contrast, contemporary drug development focuses on identifying synergistic pharmacological interactions among drugs when creating new combination therapies (Al-Lazikani et al., 2012; Chou, 2010; Han et al., 2017; Lehar et al., 2009; Rationalizing combination therapies, 2017; Sun et al., 2013).

In this paper we directly assess pharmacological interaction and cross-resistance among the drugs comprising R-CHOP, a highly successful curative cancer therapy developed over the course of decades by experimentation in patients with DLBCL. When tested in three DLBCL cell lines over a wide range of drug concentrations, we observed no significant synergy among R-CHOP constituents using either Bliss Independence or Loewe Additivity criteria: pairwise drug interactions ranged from additive to antagonistic, and the combined activity of all 5 drugs was close to purely additive. The significance of antagonism among some drug pairs is not clear but studies of antibiotics have shown that antagonistic drug interactions can suppress the emergence of drug-resistant mutants (Chait et al., 2007; Michel et al., 2008; Yeh et al., 2009).

We investigated the frequencies and mechanisms of resistance to R-CHOP using DNA barcoding and CRISPRi/a technology. These three approaches made it possible to explore drug resistance and cross-resistance caused by point mutations, chromosome aberrations, and increased or decreased gene dosage. Large library size (10^6 clones) is a strength of the barcoding approach and it yielded $>10^4$ DLBCL mutants resistant to one or more drugs (as measured in biological triplicate). Genome-wide CRISPRi/a screening is more challenging technically, but it provided the capability to pinpoint hundreds of individual genes involved in resistance and sensitivity. The results of all three resistance screens were

clear: progressively fewer clones were observed with resistance to one, two, three or four drugs. The frequencies of multi-drug resistance were close to the theoretical minimum, as defined by the product of empirically determined frequencies of single-drug resistance. The existence of multi-drug resistance mechanisms (such as transporter overexpression) was responsible for the slight increase in cross-resistance over the theoretical minimum, but their impact was relatively modest because multi-drug resistance was rarer than single-drug resistance, and generally applied to a subset of drugs, not to all. Our data therefore confirm the hitherto untested theories of Law and Frei (Frei et al., 1965; Law, 1952).

The current work was performed in cultured cells and it is likely that the components of R-CHOP have additional mechanisms of action in human patients. For example, rituximab is cytotoxic to DLBCL by signaling-induced cell death, complement-mediated cytotoxicity (CMC), and antibody dependent cellular cytotoxicity (ADCC) (Weiner, 2010). In this study we only score CMC since DLBCL cultures displayed little direct induction of apoptosis, and ADCC reconstituted *in vitro* using peripheral blood mononuclear cells elicits insufficient cell death for selection of resistant clones (typically less than 50% killing) (Dall'Ozzo et al., 2004; Reff et al., 1994). We cannot exclude the possibility that ADCC interacts synergistically with chemotherapy but note that the immunosuppressive effects of many chemotherapies disfavor this hypothesis. With regard to the evolution of drug resistance, Rituximab may behave as though it is several drugs in one due to its multiple mechanisms, although CD20 loss would constitute a shared cause of resistance (Figure 9A). Prednisone, the pro-drug of prednisolone, can induce remissions of DLBCL even as a single agent (Lamar, 2016), although cytotoxicity was not evident in cell cultures. Cell culture is nonetheless an appropriate setting in which to test the Law and Frei hypothesis: such a test requires molecular manipulations and phenotypic screens over wide dose ranges that can only be performed in culture, and evidence that an animal model (or patient) benefits from combination therapy does not discriminate among alternative mechanisms of benefit. Moreover, the

assessment of synergistic interactions in new drug combinations is most often performed in culture, making our analysis of interactions in R-CHOP directly relevant.

In their 1964 study on the curability of experimental leukemia, Skipper, Schabel, and Wilcox observed that a given dose of alkylating chemotherapy kills a fixed fraction of cancer cells regardless of population size (equivalently, the logarithm of the number of cancer cells is reduced by a fixed quantity) (Skipper et al., 1964). 'Fractional kill', also called 'log kill', has been observed for many cancer therapies and is thought to reflect the impact of genetic and phenotypic heterogeneity on drug response (Paek et al., 2016; Spencer et al., 2009). Considered in the context of combination therapy, the number of 'log kills' contributed by each drug is expected to be arithmetically additive if the drugs have different resistance mechanisms, precisely as we have observed for R-CHOP (Figure 9A). For example, if each of two drugs induce 99% kill (2 log-kills), and the 1% surviving fractions overlap by no more than chance, as occurs with low cross-resistance, then only 1% of 1% of cancer cells will survive both drugs used in combination, resulting in 99.99% kill (2 + 2 = 4 log-kills). Thus, combinations of individually effective drugs with low cross-resistance can achieve high fractional tumor cell killing despite a lack of synergistic drug interaction. Enhanced fractional kill can equivalently be understood from a pharmacological perspective. As discussed above, the dose response of DLBCL to R-CHOP is very close to additive, which is nonetheless a basis for therapeutic superiority over monotherapy. Because toxicities limit the maximum dose of each single agent, when the constituents of a combination have qualitatively different toxicities (as in R-CHOP) (Neal and Hoskin, 2009) they can be administered simultaneously at close to maximum tolerated doses. The result of a higher 'sum of dose intensities' (Frei et al., 1998) is precisely what is predicted based on the fractional cell kill model, if it can be achieved at acceptable toxicity.

The results of this paper do not suggest that drug additivity and low cross-resistance are necessarily sufficient for cure: what is critical in an additive drug combination are the absolute

magnitudes of each drug's effect. Because of the large numbers of cancer cells often present in DLBCL at the time of diagnosis ($>10^{10}$), it is logical to presume that in a combination such as R-CHOP each drug must contribute 2-3 log kills, on average, to achieve a cure. It remains unclear whether a cure requires that a chemotherapy regimen eradicate every cancer cell or if the immune system can clear malignant diseases when cell number falls below some threshold (Frei, 1972). The conclusions in the current paper are agnostic with respect to this important issue. Moreover, across a population of patients, the absolute magnitude of each drug's effect is expected to vary, as does initial tumor size. In Figure 9B we schematize the concepts of (i) inter-patient variability in drug response and (ii) addition of log-kills of different magnitudes. These concepts are consistent with the historical facts that some cases of DLBCL are curable with 3 drugs (CVP), more are cured with 4 drugs (CHOP) and yet more with 5 (R-CHOP); but even with the best available therapy some patients are still not cured. Adding new agents to R-CHOP has proven challenging, and before Ritixumab the 7-drug 'ProMACE-CytaBOM' regimen failed to improve DLBCL survival relative to CHOP (Fisher et al., 1993). The reasons for this are likely to be multi-faceted: some drugs may be ineffective in many patients; they may have overlapping toxicities leading to dose reductions and interruptions that compromise efficacy (Cabanillas, 2007); and they may have overlapping resistance with standard therapies such that they fail to achieve greater fractional kill.

A limitation of all tests for pharmacological interaction is they typically pertain to doses near the IC_{50} value and are therefore relevant to the most drug-susceptible part of a cell population. The primary obstacle to cure in most settings is thought to be acquired drug resistance caused by rare resistance mutations, which can arise even at very high doses. Unfortunately, systematic analysis of cross-resistance is very difficult using conventional cell culture techniques (Law, 1956), perhaps explaining why the 'non-overlapping resistance' hypothesis has not been extensively explored in pre-clinical drug development. The introduction of clone tracing and genome-wide CRISPR technologies fundamentally

changes the situation: using these methods cross-resistance can easily be studied for any new combination therapy active in cultured cells. Moreover, resistance screening is performed on individual drugs and cross-resistance is identified in a subsequent computational comparison, which makes the approach inherently scalable to many drugs and many combinations. Clone tracing has been proposed as a general approach to identifying combination regimens with non-overlapping resistance (Bhang et al., 2015). Our findings supports this proposal and suggest that screening for cross-resistance should become as routine in pre-clinical cancer pharmacology as screening for pharmacological interaction.

Acknowledgments: We thank F. Stegmeier and C. Bhang for ClonTracer, A. Letai and A. Eberly Puleo for rituximab, and also M. Chung, L. Albacker, L. Maliszewski, M. Cokol, S. Chopra, and K. Subramanian for helpful discussions.

Funding: This work was supported by NHMRC Early Career Fellowship (to A.C.P.), NIH grant P50-GM107618 and U54-CA225088 (to P.K.S.).

Author contributions: Experiments and analysis, A.C.P. and C.C.; writing, A.C.P., C.C., and P.K.S.

Competing interests:

P.K.S is a member of the SAB or Board of Directors of Merrimack Pharmaceuticals, Glencoe Software, Applied Biomath and RareCyte Inc and has equity in these companies. In the last five years the Sorger lab has received research funding from Novartis and Merck. P.K.S. declares that none of these relationships are directly or indirectly related to the content of this manuscript. Other authors declare no competing interests.

FIGURES

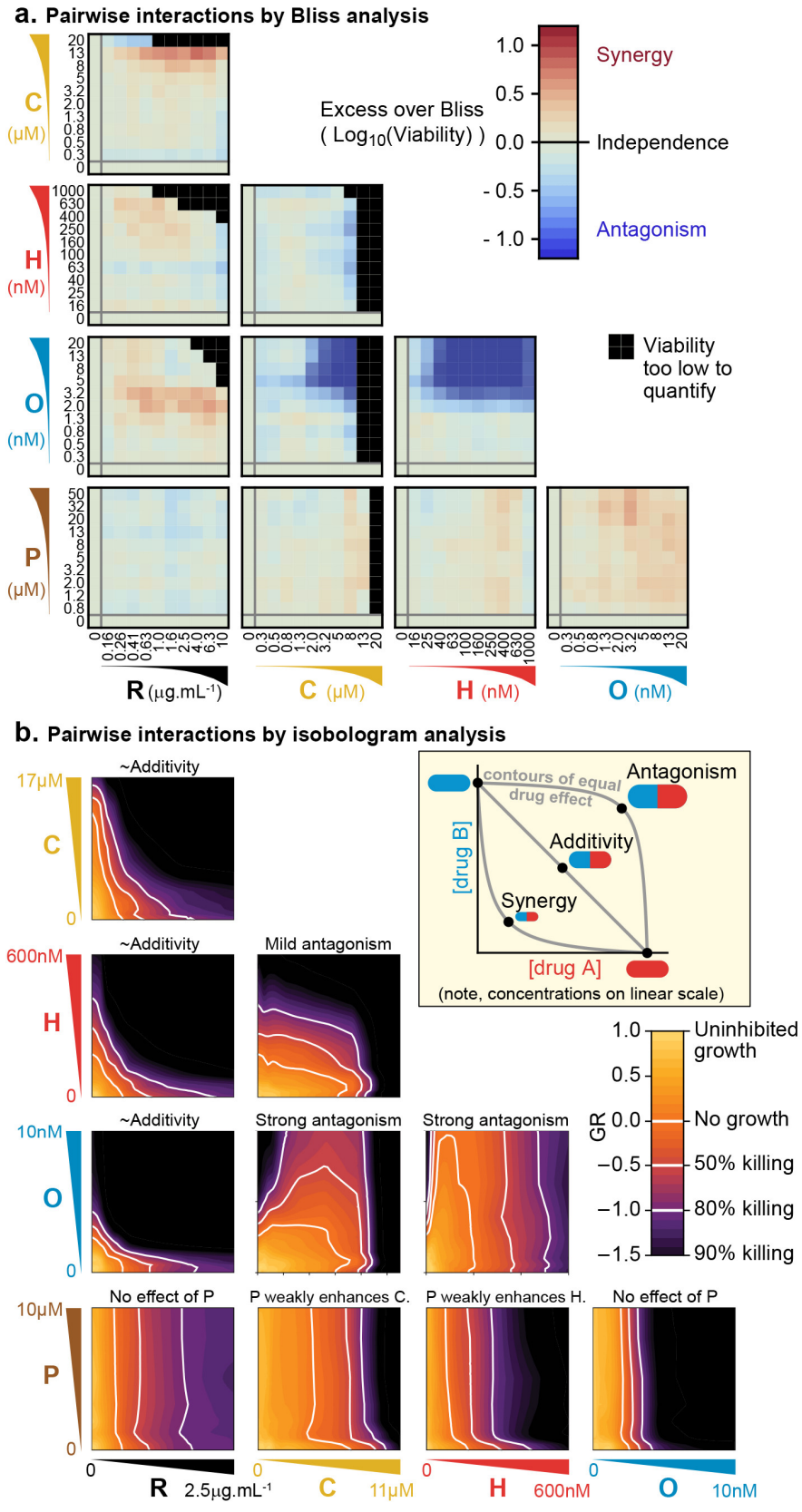

Figure 1. Pairs of drugs in R-CHOP exhibit little synergy, but some strong antagonism, in a Diffuse Large B-Cell Lymphoma cell line. a. Pfeiffer cells grown in microtiter plates were treated with drug combinations for 72 hours followed by a luminescence-based assay for cell viability. 'Excess over Bliss' measures the observed deviation from Bliss Independence. **b**. Isobologram analysis of the same experiments; luminescence relative to untreated control cells was converted into a GR metric (Hafner et al., 2016) to distinguish cytostatic from cytotoxic effects. White contours highlight thresholds equivalent to complete growth inhibition (GR = 0), and complete growth inhibition plus 50% or 80% cell killing (GR<0). Inset: principles of isobologram analysis; isoboles are contours of equal drug effect, which are straight lines in the case of 'additivity'. See also Figure S1.

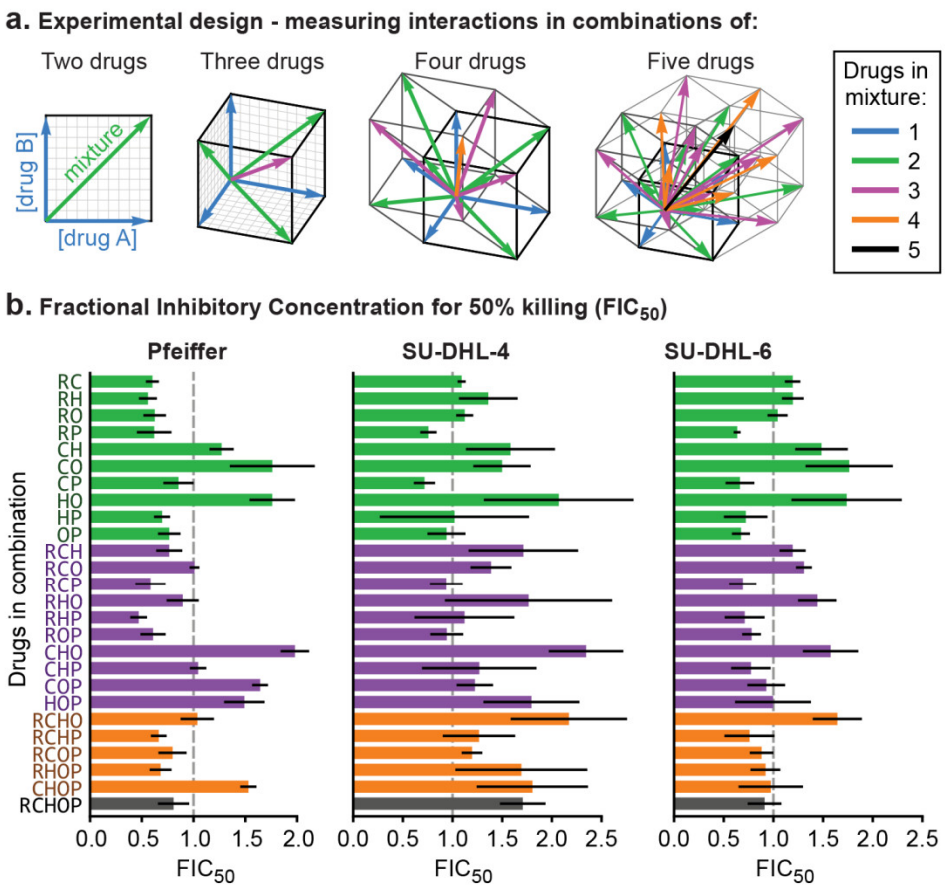

Figure 2. Higher order drug combinations do not exhibit synergistic cell killing. a. Experimental design: two or more drugs were mixed in equipotent ratios such that they similarly contributed to cytotoxicity as the dose of the mixture was increased. Dose gradients of drug mixtures span diagonal lines in multi-drug concentration space. **b**. Synergy or antagonism of multidrug combinations was quantified by Fractional Inhibitory Concentrations (FIC) at the 50% killing threshold (Figure S1D). Error bars are 95% confidence intervals (n = 4 per point along dose response). **c**. Average dose response functions to single drugs or mixtures of different numbers of drugs (i.e., average of single-drug responses; average of drug pair responses, etc.). Red line: expected response to R-CHOP drugs according to the Bliss Independence model; pale red area: ±10% error in number of log-kills around the Bliss Independence model. Top left: Horizontal axis shows the amount of each drug present in a mixture (units are scaled to align single-agent activity; Figure S2A). Top right, bottom left, bottom right: Horizontal axis is the sum of drug concentrations. See also Figure S2.

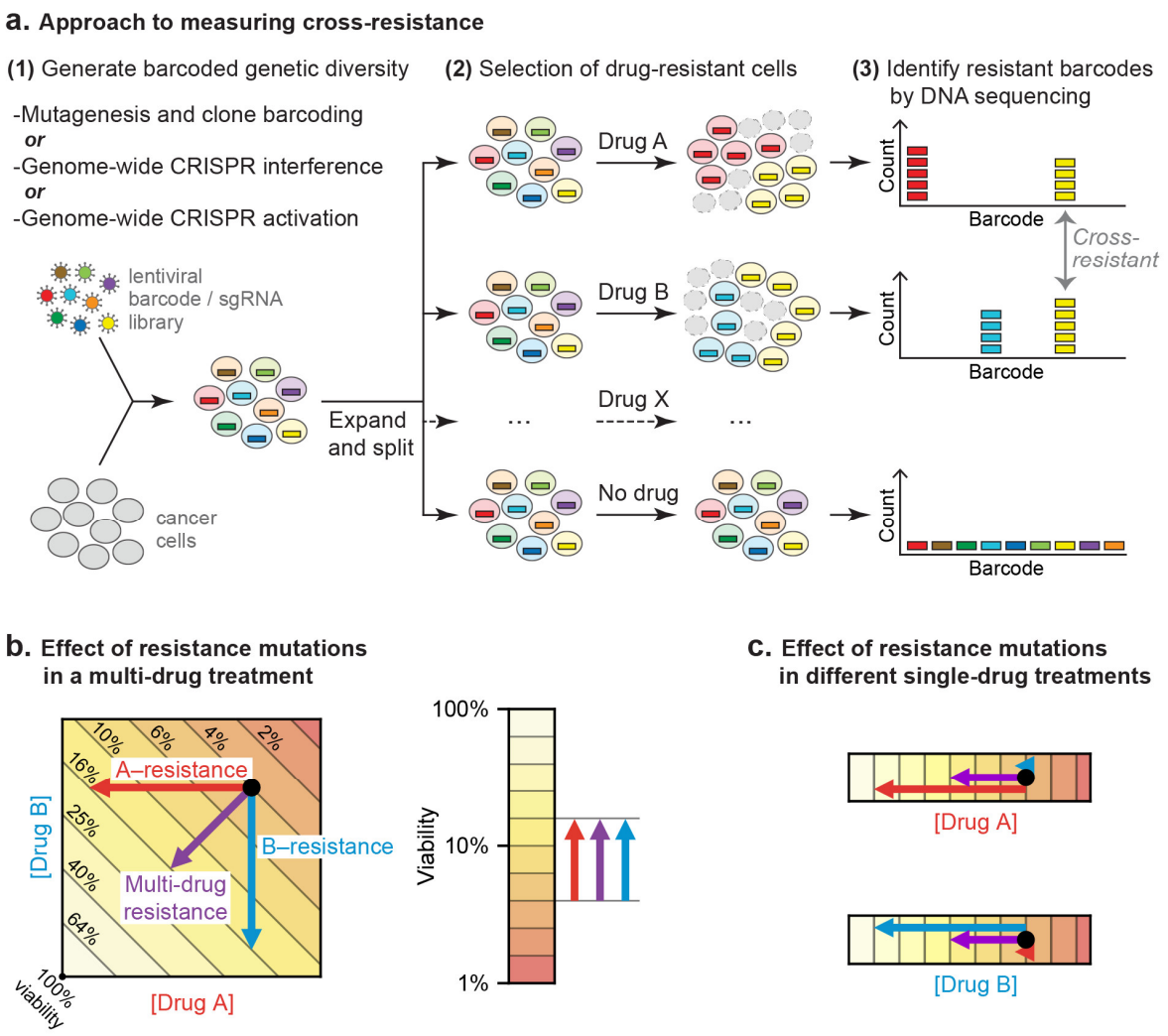

Figure 3. Strategy for measuring cross-resistance between drugs. a. Cells were mutagenized and barcoded using one of three approaches: (i) random mutagenesis and clone tracing, (ii) knockdown by CRISPRi or (iii) overexpression by CRISPRa. 10^6 mutagenized clones or genome-wide CRISPRi/a libraries were expanded and split into replicate cultures, treated with single drugs, and DNA barcodes/sgRNAs abundance was measured by DNA sequencing. The resistance of cells to drug treatment was scored based on the degree of barcode enrichment, and cross-resistance was determined by significant enrichment in two or more drug treatments. **b**. Schematic showing importance of selecting for resistance to single drugs not cocktails. Arrows: resistance is analogous to lower drug concentration and moves cells to different coordinates; cross-resistance (purple arrow) has same net effect as more

penetrant single-drug resistance mutations (red, blue arrows). **c**. By selecting mutations on single drugs the magnitude of the effect on each drug is known. See also Figure S3.

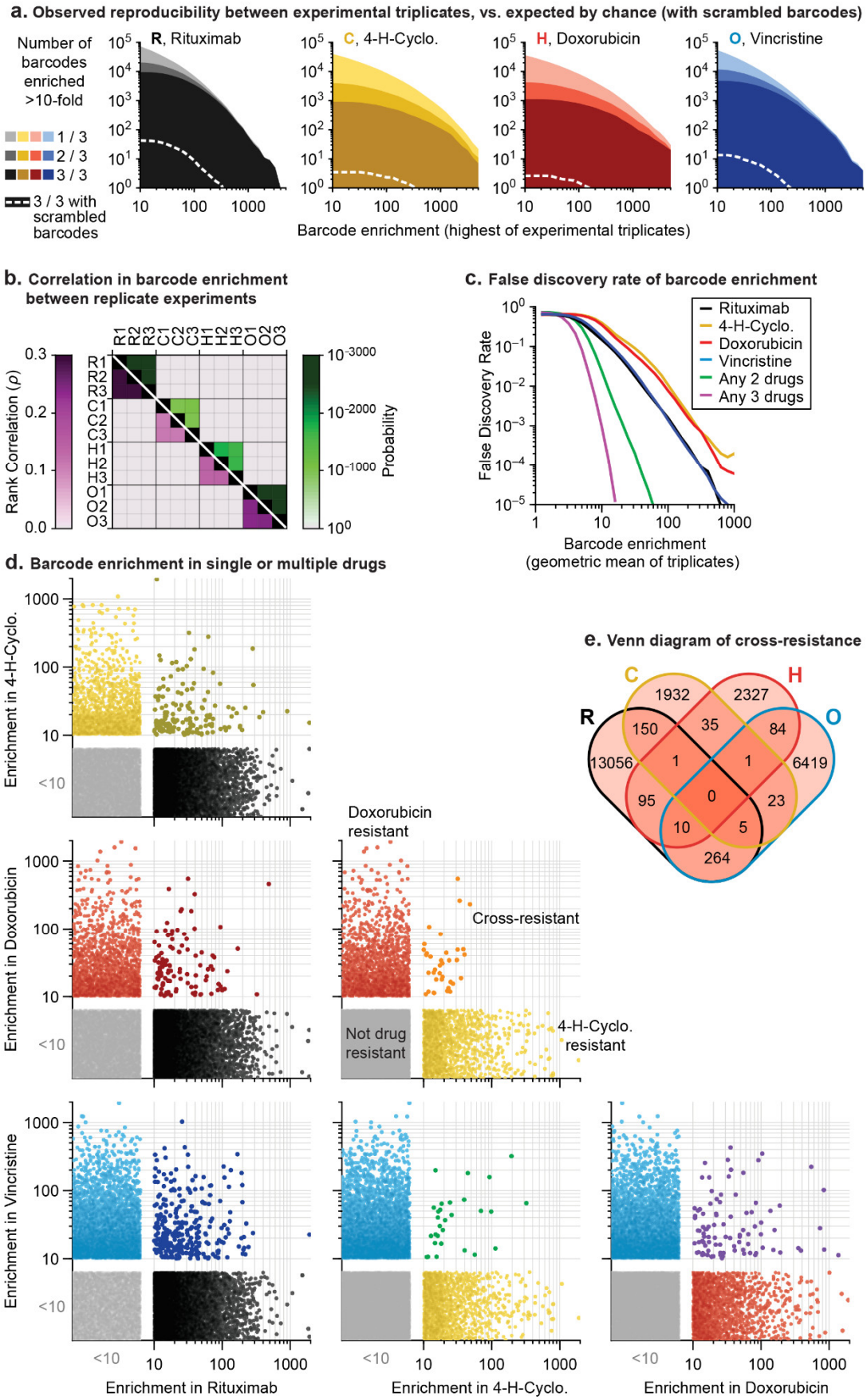

Figure 4. In mutagenized clones single-drug resistance is common but multi-drug resistance rare.

a. Reproducibility of DNA barcode enrichment among triplicate drug treatments. Horizontal axis is the highest value for each barcode's enrichment scores in any replicate. Vertical axis is the number of barcodes for which 1, 2, or 3 triplicates had enrichment ≥ 10. Dashed white line: error model indicating repeated enrichment expected by random chance; see Methods. **b**. Matrix of Spearman rank correlation in enrichment scores between drug treatments (ρ in pink scale; one-sided p-value in green scale). **c**. False discovery rate of barcode enrichment, per magnitude of enrichment (geometric mean of triplicates), was computed by comparing observed barcode enrichment to an error model of scrambled barcodes (10^{10} triplicates simulated by scrambling actual data). At geometric mean enrichment = 10, false discovery rate for 2-drug and 3-drug resistance is 2.5% and 0.1%, respectively. **d.** Scatterplots of barcode enrichment scores (geometric mean of biological triplicates for each drug) for each pair of two drugs in RCHO. Each dot represents a single barcode. Enrichment scores < 10 are deemed not significant. **e**. Venn diagram of the number of barcodes exhibiting resistance (geometric mean enrichment ≥ 10) to single or multiple drugs. See also Figure S4.

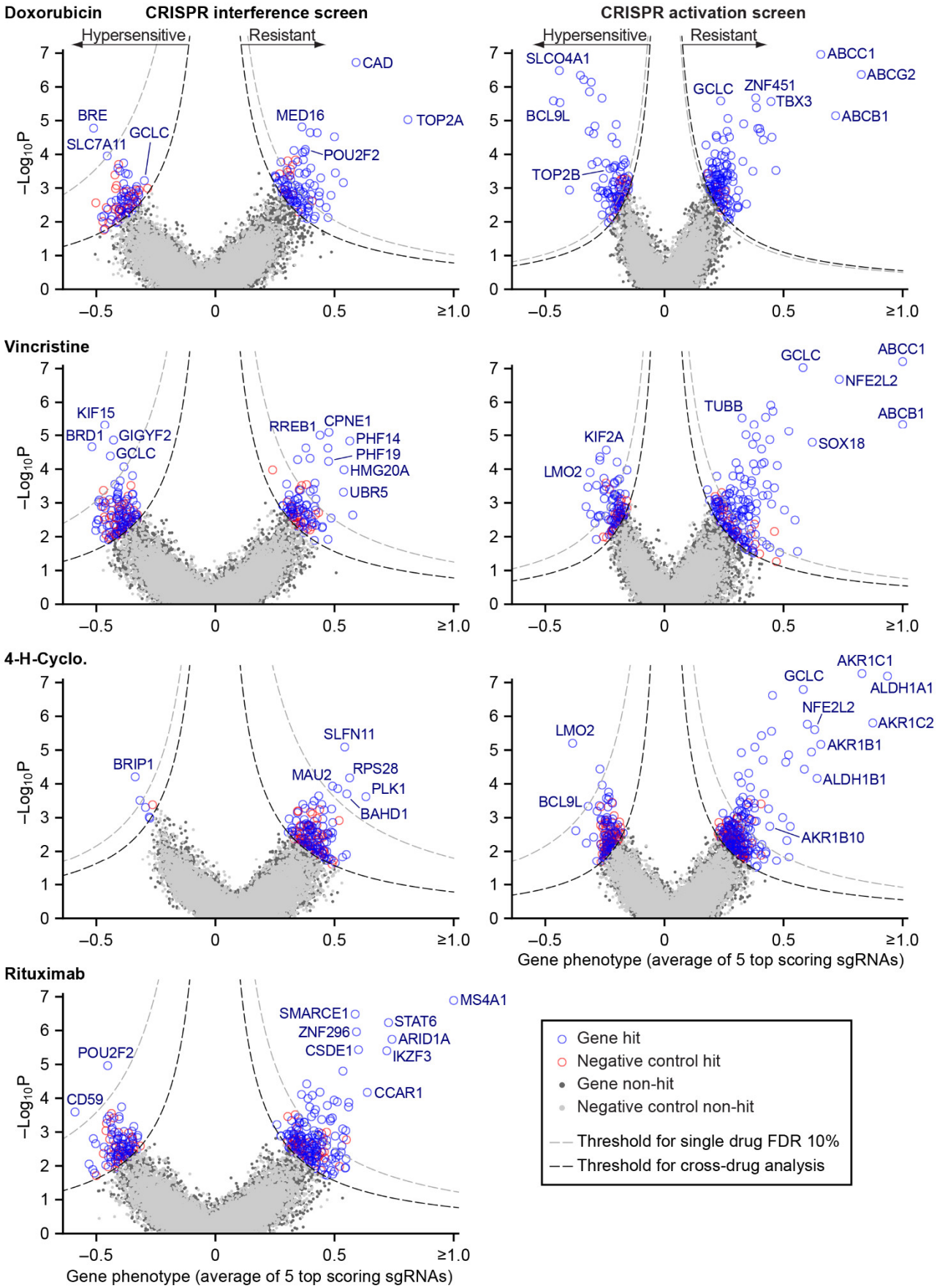

Figure 5. Identification of mechanisms of single drug resistance by genome-wide CRISPRi and CRISPRa screening. Volcano plots of gene phenotype and p-value for CRISPRi (left) and CRISPRa (right) screens of single R-CHOP drugs. Phenotype of 1 is full resistance, 0 is parental sensitivity, <0 is hypersensitivity. The coordinate of each gene was determined by the average phenotype of the 5 most active sgRNAs targeting that gene and $-\log_{10}$ of the p-value (Mann-Whitney test of phenotypes for all targeting sgRNAs compared to 4,000 non-targeting controls). Negative control genes were generated by randomly grouping sets of non-targeting sgRNAs. Gray dashed line: threshold for 10% FDR for single-drug resistance, or hypersensitivity. Black dashed line: threshold for cross-resistance set to yield less than one double-resistant negative control gene out of all possible drug pairs (equal to multi-drug resistance FDR 4% for CRISPRi and 2% for CRISPRa). Labeled genes are a partial list of top scoring hits. See also Figure S5.

a. CRISPR i screen validation

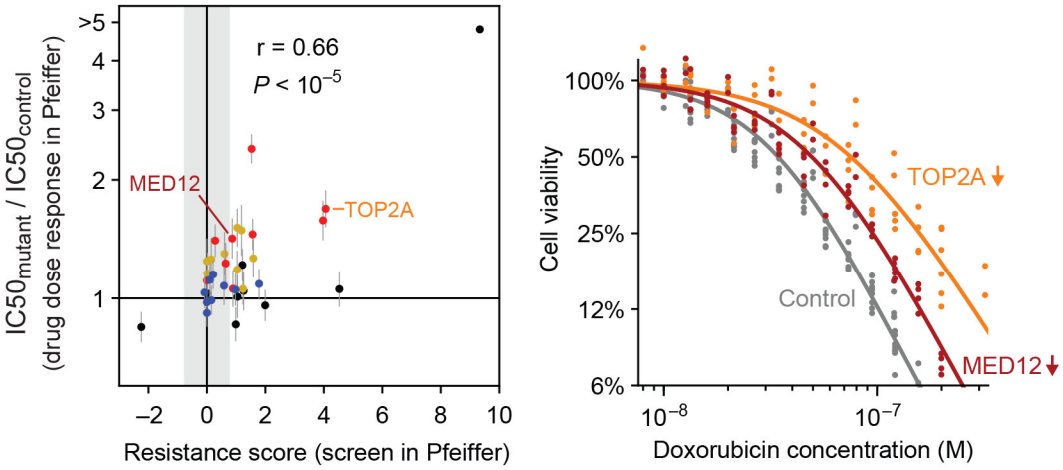

b. CRISPR a screen validation (K562)

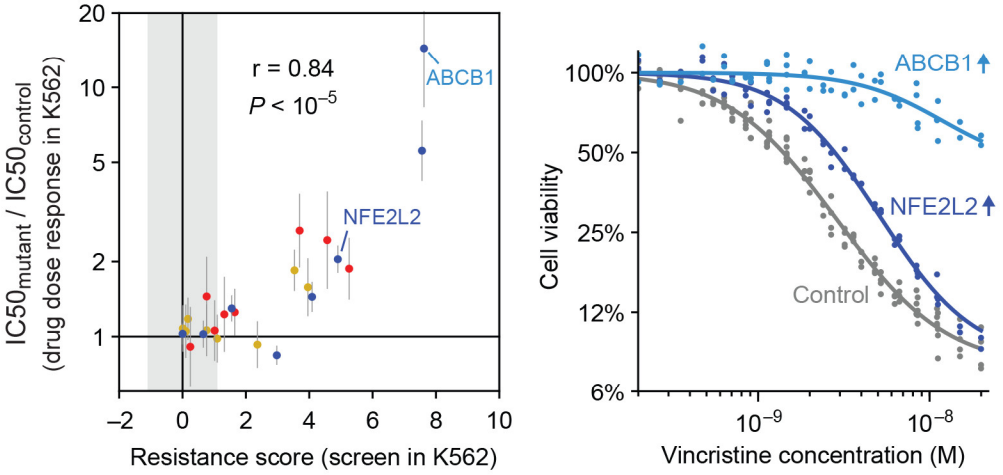

c. CRISPR a screen validation (Pfeiffer)

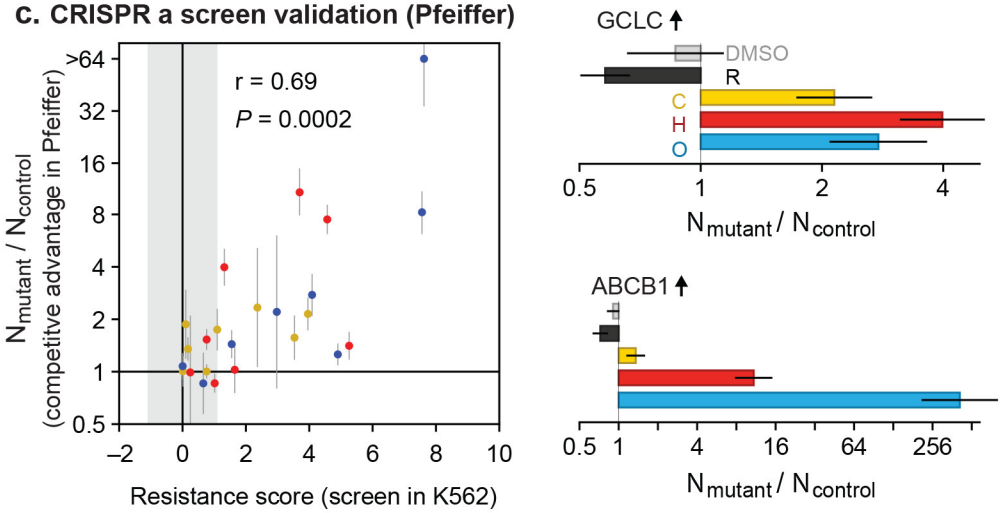

Figure 6. Validation of CRISPRi and CRISPRa screen results by individual drug sensitivity measurements. a. Gene knockdown by CRISPRi produces changes in drug sensitivity (IC50) that are correlated with resistance phenotypes from the genome-wide CRISPRi screen (Pearson correlation r = 0.66, $P < 10^{-5}$). Drug dose responses were measured in Pfeiffer CRISPRi cells bearing single sgRNAs, for each of 9 knockdown screen hits, or control non-targeting sgRNA. Error bars are 95% confidence intervals in IC50 (determined from curve fit; n=6). Point color indicates drug: black, rituximab; yellow, 4-HC; red, doxorubicin; blue, vincristine. Gray region: threshold in resistance score that was used to identify screen hits. Right: example dose response measurements for control sgRNAs, or sgRNAs inducing *TOP2A* and *MED12* knockdown and consequent doxorubicin resistance. **b.** Gene overexpression by CRISPRa produces changes in drug sensitivity (IC50) that are correlated with resistance phenotypes from the genome-wide CRISPRa screen (r = 0.84, $P < 10^{-5}$). Drug dose responses (n=4) were measured in K562 CRISPRa cells bearing sgRNAs for each of 8 overexpression screen hits, or control non-targeting sgRNA. Right: example dose response measurements for control sgRNAs, or sgRNAs inducing overexpression of *ABCB1* and *NFE2L2* and consequent vincristine resistance. **c.** Gene overexpression by CRISPRa in DLBCL cells (Pfeiffer) produces drug resistance that is correlated with resistance scores from the CRISPRa screen in K562 cells (r = 0.69, $P = 0.0002$). Pfeiffer CRISPRa cells bearing targeted sgRNAs were mixed at 1:1 ratio with cells bearing non-targeting sgRNA, the co-culture was subjected to two 72 hour drug treatment and recovery periods, and changes in the ratio of mutant to control cells was measured by qPCR of sgRNAs. Error bars are 95% confidence intervals (n=3). Right: Change in ratio of cells bearing sgRNA that induces *GCLC* overexpression (or *ABCB1* overexpression) versus cells bearing control sgRNA, after drug treatment. See also Figure S6.

a. **Cross-resistance among gene knockdown mutants (CRISPRi)**

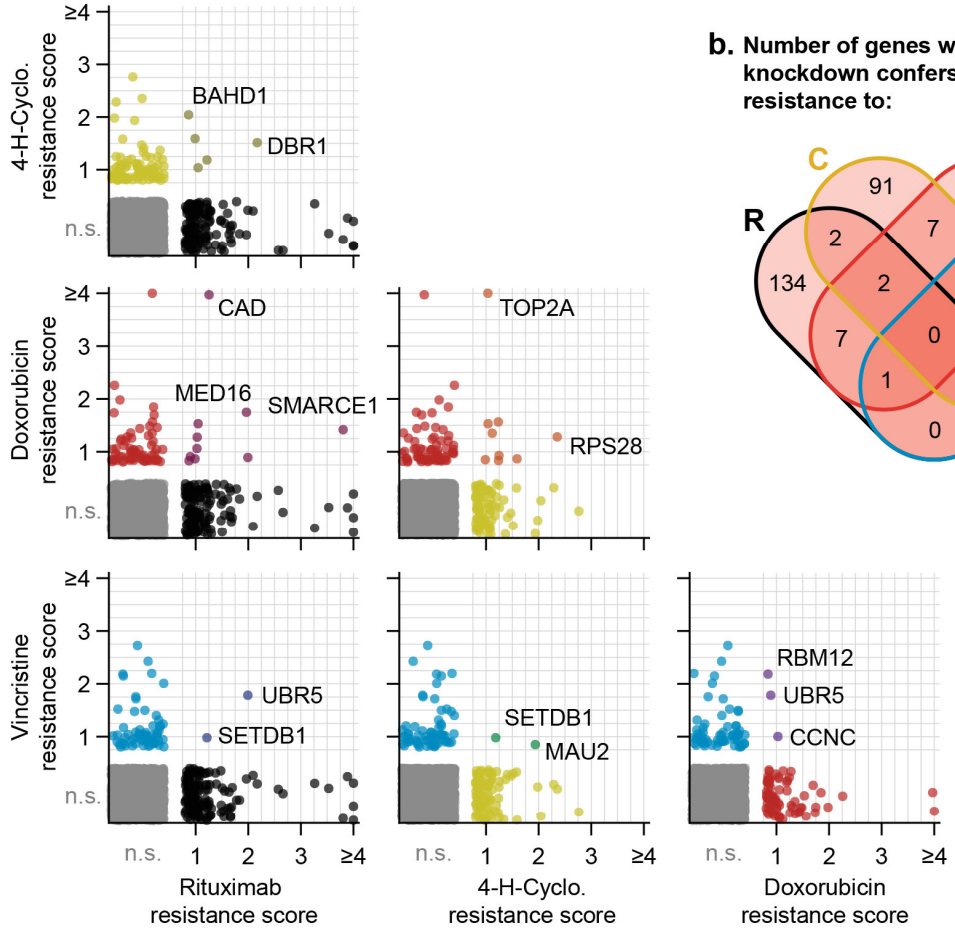

b. **Number of genes whose knockdown confers resistance to:**

c. **Cross-resistance among gene overexpression mutants (CRISPRa)**

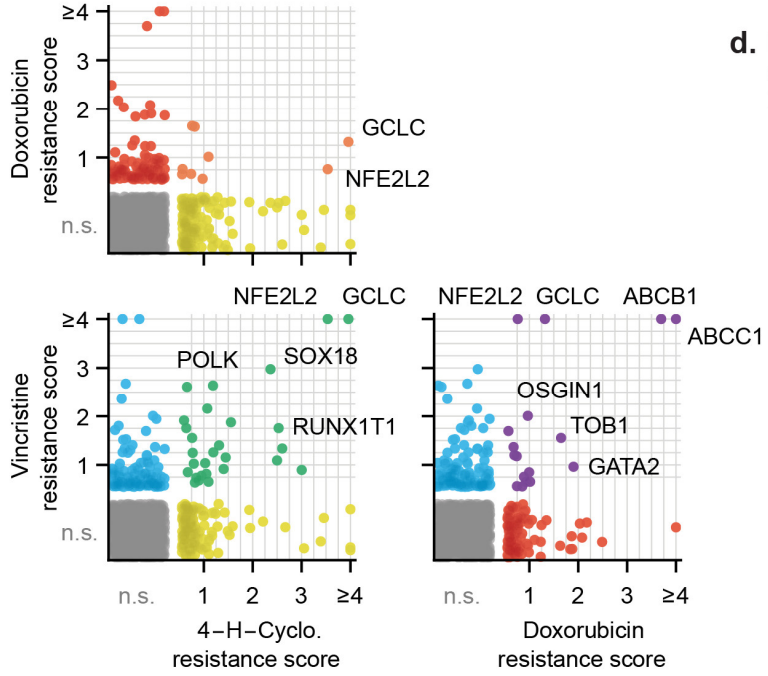

d. **Number of genes whose overexpression confers resistance to:**

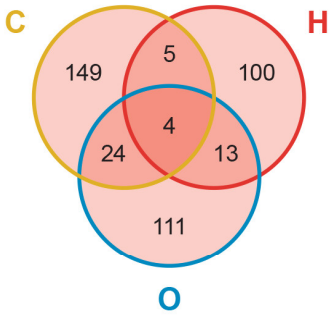

Figure 7. Cross-resistance analysis of the CRISPRi and CRISPRa screens reveals a small number of multi-drug resistance mechanisms. a. Scatter plots of resistance scores obtained in CRISPRi screens for each pair of drugs in RCHO; each dot represents a gene. Resistance scores were calculated from the product of the gene phenotype and the significance of the enrichment ($-\log_{10}P$). n.s., not significant; genes significant in one drug treatment but not in another are displayed against the left or bottom axis. Labeled genes are a partial list of top scoring hits. **b.** Venn diagram of the number of genes whose knockdown confers resistance to one or multiple drugs in RCHO. **c.** Scatter plots of resistance scores obtained in CRISPRa screens for each pair of drugs in CHO. Data were analyzed and displayed as in (**a**). **d.** Venn diagram of the number of genes whose overexpression confers resistance to one or multiple drugs in CHO. See also Figures S7 and S8.

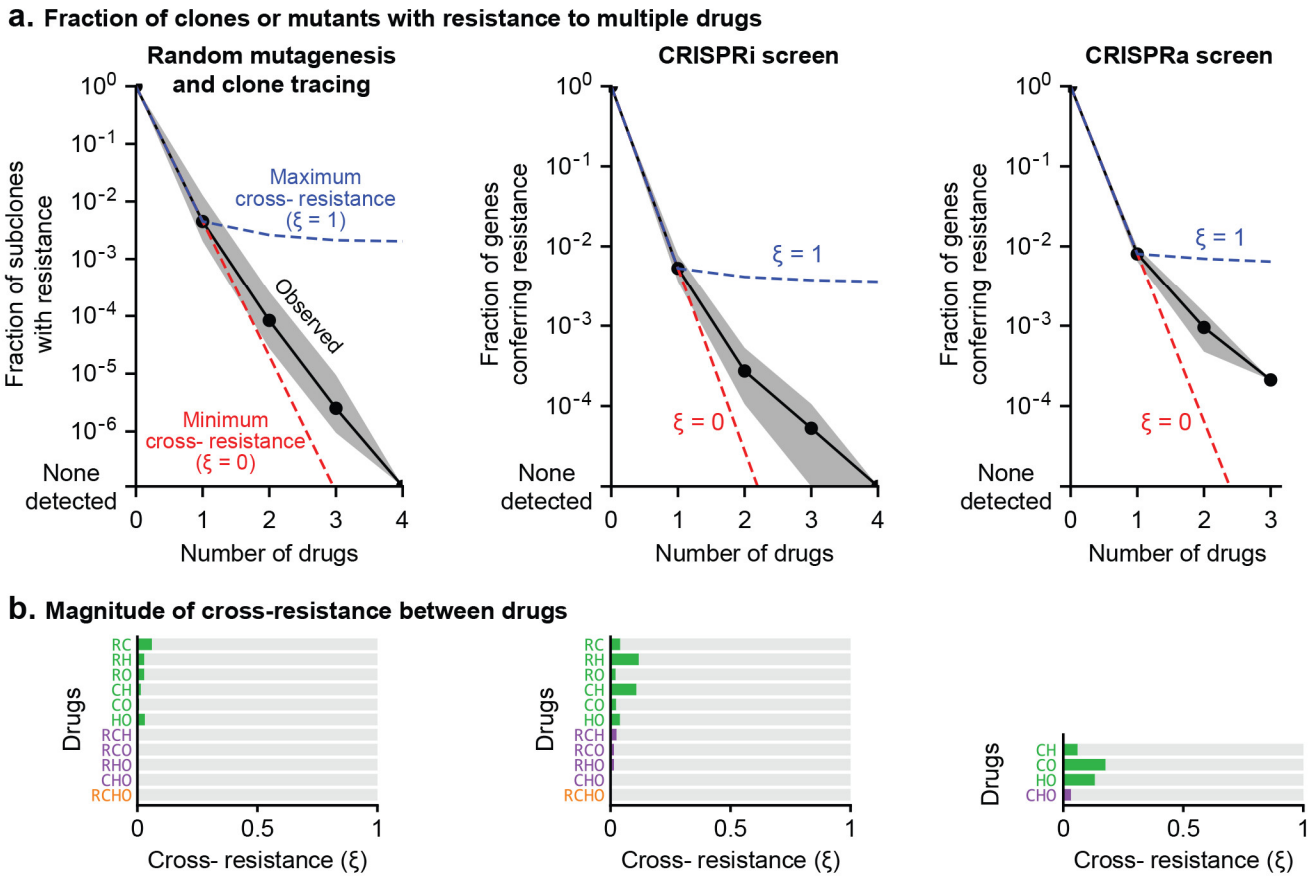

Figure 8. Cross-resistance between drugs in R-CHOP is close to its theoretical minimum. a. Fraction of clones or genetic perturbations resistant to one or more drugs in RCHO. Gray shading spans the range for different sets of drugs (e.g. 6 different pairs), and black points mark the average on a log scale. Dashed blue line: average frequency of Multi-Drug Resistance (MDR) if resistance is maximally overlapping (maximal overlap is the minimum of constituent single drug MDR frequencies; cross resistance parameter $\xi = 1$). Dashed red line: average frequency of MDR as the product of single-drug MDR frequencies with $\xi = 0$. **b**. Strength of cross-resistance (ξ) for different sets of drugs in RCHO, as determined from data summarized in (**a**).

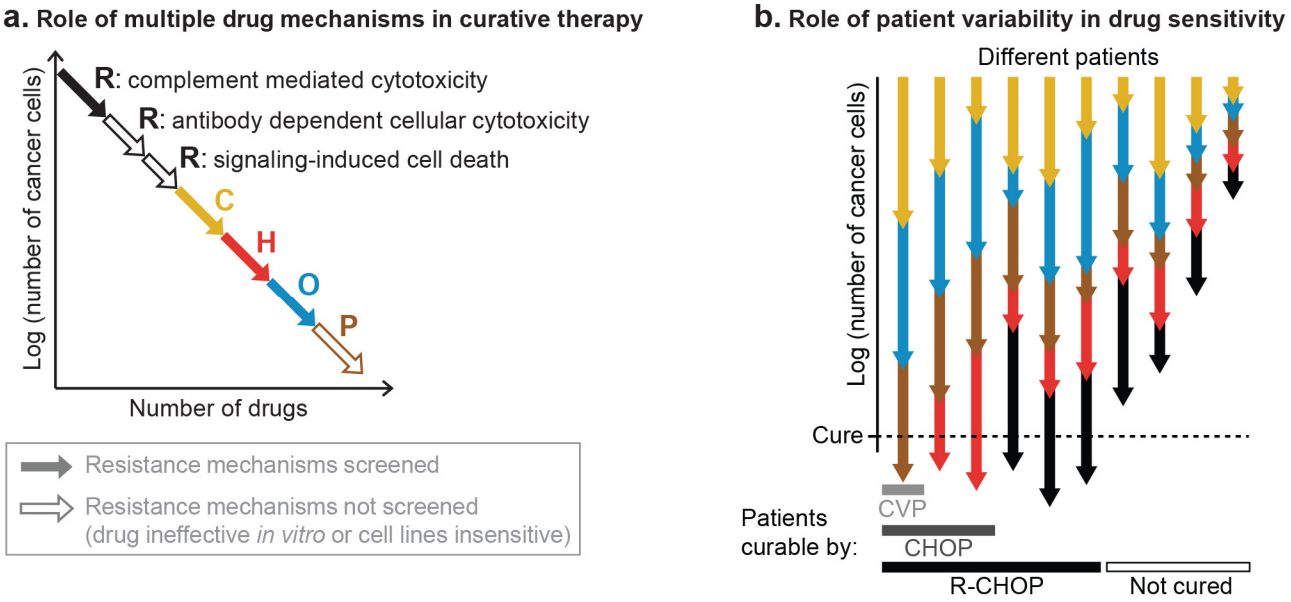

Figure 9. The role of multiple drug mechanisms in increasing the probability of cure by combination therapy. a. Conceptual schematic of the role of multiple drug mechanisms, each subject to different mechanisms of resistance, in the eradication of drug resistant clones and cure of a patient's cancer. When cross-resistance is low, the 'log-kills' achieved by each drug mechanism add up. **b**. Conceptual schematic of the role of patient-to-patient variability in sensitivity to each drug. Addition of 'log-kills' does not guarantee they will add up to enough to cure all patients, or even any; the effect of combination therapy in each patient depends on the magnitude of effect of each constituent drug, which varies across patients. Consistent with the clinical history of DLBCL, larger numbers of individually potent and non-cross-resistant therapies is expected to increase the fraction of patients cured. It remains unresolved whether chemotherapy must eradicate every cancer cell.

SUPPLEMENTAL DATA

Document S1. Figures S1–S8, Tables S1 and S2

Table S3. Barcode counts for all clone tracing experiments. Related to Figure 4.

Table S4. sgRNA counts for all CRISPRi screens. Related to Figure 5.

Table S5. sgRNA counts for all CRISPRa screens. Related to Figure 5.

Table S6. sgRNA phenotype scores for all CRISPRi screens. Related to Figure 5.

Table S7. sgRNA phenotype scores for all CRISPRa screens. Related to Figure 5.

Table S8. Gene scores for all CRISPRi screens. Related to Figure 5.

Table S9. Gene scores for all CRISPRa screens. Related to Figure 5.

REFERENCES

Alizadeh, A.A., Eisen, M.B., Davis, R.E., Ma, C., Lossos, I.S., Rosenwald, A., Boldrick, J.C., Sabet, H., Tran, T., Yu, X., Powell, J.I., Yang, L., Marti, G.E., Moore, T., Hudson, J., Lu, L., Lewis, D.B., Tibshirani, R., Sherlock, G., Chan, W.C., Greiner, T.C., Weisenburger, D.D., Armitage, J.O., Warnke, R., Levy, R., Wilson, W., Grever, M.R., Byrd, J.C., Botstein, D., Brown, P.O., Staudt, L.M., 2000. Distinct types of diffuse large B-cell lymphoma identified by gene expression profiling. Nature 403, 503–11. https://doi.org/10.1038/35000501

Al-Lazikani, B., Banerji, U., Workman, P., 2012. Combinatorial drug therapy for cancer in the post-genomic era. Nat Biotechnol 30, 679–92. https://doi.org/10.1038/nbt.2284

Andreadis, C., Gimotty, P.A., Wahl, P., Hammond, R., Houldsworth, J., Schuster, S.J., Rebbeck, T.R., 2007. Members of the glutathione and ABC-transporter families are associated with clinical outcome in patients with diffuse large B-cell lymphoma. Blood 109, 3409–16. https://doi.org/10.1182/blood-2006-09-047621

Bansal, A., Simon, M.C., 2018. Glutathione metabolism in cancer progression and treatment resistance. J Cell Biol 217, 2291–2298. https://doi.org/10.1083/jcb.201804161

Barlogie, B., Drewinko, B., Johnston, D.A., Freireich, E.J., 1976. The effect of adriamycin on the cell cycle traverse of a human lymphoid cell line. Cancer Res 36, 1975–9.

Berenbaum, M.C., 1989. What is synergy? Pharmacol Rev 41, 93–141.

Bhang, H.E., Ruddy, D.A., Krishnamurthy Radhakrishna, V., Caushi, J.X., Zhao, R., Hims, M.M., Singh, A.P., Kao, I., Rakiec, D., Shaw, P., Balak, M., Raza, A., Ackley, E., Keen, N., Schlabach, M.R., Palmer, M., Leary, R.J., Chiang, D.Y., Sellers, W.R., Michor, F., Cooke, V.G., Korn, J.M., Stegmeier, F., 2015. Studying clonal dynamics in response to cancer therapy using high-complexity barcoding. Nat Med 21, 440–8. https://doi.org/10.1038/nm.3841

Bliss, C.I., 1939. The toxicity of poisons applied jointly. Ann. Appl. Biol. 26, 585–615.

Bozic, I., Reiter, J.G., Allen, B., Antal, T., Chatterjee, K., Shah, P., Moon, Y.S., Yaqubie, A., Kelly, N., Le, D.T., Lipson, E.J., Chapman, P.B., Diaz, L.A., Vogelstein, B., Nowak, M.A., 2013. Evolutionary dynamics of cancer in response to targeted combination therapy. Elife 2, e00747. https://doi.org/10.7554/eLife.00747

Cabanillas, F., 2007. Dose dense CHOP: when more is not always better! Leuk. Lymphoma 48, 845–846. https://doi.org/10.1080/10428190701321285

Chait, R., Craney, A., Kishony, R., 2007. Antibiotic interactions that select against resistance. Nature 446, 668–71. https://doi.org/10.1038/nature05685

Choi, C.H., 2005. ABC transporters as multidrug resistance mechanisms and the development of chemosensitizers for their reversal. Cancer Cell Int 5, 30. https://doi.org/10.1186/1475-2867-5-30

Chou, T.C., 2010. Drug combination studies and their synergy quantification using the Chou-Talalay method. Cancer Res 70, 440–6. https://doi.org/10.1158/0008-5472.CAN-09-1947

Cokol, M., Kuru, N., Bicak, E., Larkins-Ford, J., Aldridge, B.B., 2017. Efficient measurement and factorization of high-order drug interactions in Mycobacterium tuberculosis. Sci. Adv. 3. https://doi.org/10.1126/sciadv.1701881

Cox, P.J., Phillips, B.J., Thomas, P., 1975. The enzymatic basis of the selective action of cyclophosphamide. Cancer Res 35, 3755–61.

Cutts, J.H., 1961. The effect of vincaleukoblastine on dividing cells in vivo. Cancer Res 21, 168–72.

Dall'Ozzo, S., Tartas, S., Paintaud, G., Cartron, G., Colombat, P., Bardos, P., Watier, H., Thibault, G., 2004. Rituximab-dependent cytotoxicity by natural killer cells: influence of FCGR3A polymorphism on the concentration-effect relationship. Cancer Res 64, 4664–9. https://doi.org/10.1158/0008-5472.CAN-03-2862

Davidoff, A.N., Mendelow, B.V., 1993. Cell-cycle disruptions and apoptosis induced by the cyclophosphamide derivative mafosfamide. Exp Hematol 21, 922–7.

de Jonge, M.E., Huitema, A.D., Rodenhuis, S., Beijnen, J.H., 2005. Clinical pharmacokinetics of cyclophosphamide. Clin Pharmacokinet 44, 1135–64. https://doi.org/10.2165/00003088-200544110-00003

Eden, E., Navon, R., Steinfeld, I., Lipson, D., Yakhini, Z., 2009. GOrilla: a tool for discovery and visualization of enriched GO terms in ranked gene lists. BMC Bioinformatics 10, 48. https://doi.org/10.1186/1471-2105-10-48

Elion, G.B., Singer, S., Hitchings, G.H., 1954. Antagonists of nucleic acid derivatives. VIII. Synergism in combinations of biochemically related antimetabolites. J Biol Chem 208, 477–88.

Fisher, R.I., Gaynor, E.R., Dahlberg, S., Oken, M.M., Grogan, T.M., Mize, E.M., Glick, J.H., Coltman, C.A., Miller, T.P., 1993. Comparison of a standard regimen (CHOP) with three intensive chemotherapy regimens for advanced non-Hodgkin's lymphoma. N Engl J Med 328, 1002–6. https://doi.org/10.1056/NEJM199304083281404

Frei, E., 1972. Combination cancer therapy: Presidential address. Cancer Res 32, 2593–607.

Frei, E., Antman, K.H., 2000. Principles of Dose, Schedule, and Combination Chemotherapy, in: Bast, R.C., Kufe, D.W., Pollock, R.E., Weichselbaum, R.R., Holland, J.F., Frei, E. (Eds.), Holland-Frei Cancer Medicine. BC Decker, Hamilton (ON).

Frei, E., Elias, A., Wheeler, C., Richardson, P., Hryniuk, W., 1998. The relationship between high-dose treatment and combination chemotherapy: the concept of summation dose intensity. Clin Cancer Res 4, 2027–37.

Frei, E., Karon, M., Levin, R.H., Freireich, E.J., Taylor, R.J., Hananian, J., Selawry, O., Holland, J.F., Hoogstraten, B., Wolman, I.J., Abir, E., Sawitsky, A., Lee, S., Mills, S.D., Burgert, E.O., Spurr, C.L., Patterson, R.B., Ebaugh, F.G., James, G.W., Moon, J.H., 1965. The effectiveness of combinations of antileukemic agents in inducing and maintaining remission in children with acute leukemia. Blood 26, 642–56.

Gidding, C.E., Kellie, S.J., Kamps, W.A., de Graaf, S.S., 1999. Vincristine revisited. Crit Rev Oncol Hematol 29, 267–87.

Gilbert, L.A., Horlbeck, M.A., Adamson, B., Villalta, J.E., Chen, Y., Whitehead, E.H., Guimaraes, C., Panning, B., Ploegh, H.L., Bassik, M.C., Qi, L.S., Kampmann, M., Weissman, J.S., 2014. Genome-Scale CRISPR-Mediated Control of Gene Repression and Activation. Cell 159, 647–61. https://doi.org/10.1016/j.cell.2014.09.029

Gilbert, L.A., Larson, M.H., Morsut, L., Liu, Z., Brar, G.A., Torres, S.E., Stern-Ginossar, N., Brandman, O., Whitehead, E.H., Doudna, J.A., Lim, W.A., Weissman, J.S., Qi, L.S., 2013. CRISPR-mediated modular RNA-guided regulation of transcription in eukaryotes. Cell 154, 442–51. https://doi.org/10.1016/j.cell.2013.06.044

Goel, S., Wang, Q., Watt, A.C., Tolaney, S.M., Dillon, D.A., Li, W., Ramm, S., Palmer, A.C., Yuzugullu, H., Varadan, V., Tuck, D., Harris, L.N., Wong, K.K., Liu, X.S., Sicinski, P., Winer, E.P., Krop, I.E., Zhao, J.J., 2016. Overcoming Therapeutic Resistance in HER2-Positive Breast Cancers with CDK4/6 Inhibitors. Cancer Cell 29, 255–69. https://doi.org/10.1016/j.ccell.2016.02.006

Greco, W.R., Bravo, G., Parsons, J.C., 1995. The search for synergy: a critical review from a response surface perspective. Pharmacol Rev 47, 331–85.

Hafner, M., Niepel, M., Chung, M., Sorger, P.K., 2016. Growth rate inhibition metrics correct for confounders in measuring sensitivity to cancer drugs. Nat Methods 13, 521. https://doi.org/10.1038/nmeth.3853

Han, K., Jeng, E.E., Hess, G.T., Morgens, D.W., Li, A., Bassik, M.C., 2017. Synergistic drug combinations for cancer identified in a CRISPR screen for pairwise genetic interactions. Nat Biotechnol 35, 463–474. https://doi.org/10.1038/nbt.3834

Hata, A.N., Niederst, M.J., Archibald, H.L., Gomez-Caraballo, M., Siddiqui, F.M., Mulvey, H.E., Maruvka, Y.E., Ji, F., Bhang, H.E., Krishnamurthy Radhakrishna, V., Siravegna, G., Hu, H., Raoof, S., Lockerman, E., Kalsy, A., Lee, D., Keating, C.L., Ruddy, D.A., Damon, L.J., Crystal, A.S., Costa, C., Piotrowska, Z., Bardelli, A., Iafrate, A.J., Sadreyev, R.I., Stegmeier, F., Getz, G., Sequist, L.V., Faber, A.C., Engelman, J.A., 2016. Tumor cells can follow distinct evolutionary paths to become resistant to epidermal growth factor receptor inhibition. Nat Med 22, 262–9. https://doi.org/10.1038/nm.4040

Horlbeck, M.A., Gilbert, L.A., Villalta, J.E., Adamson, B., Pak, R.A., Chen, Y., Fields, A.P., Park, C.Y., Corn, J.E., Kampmann, M., Weissman, J.S., 2016. Compact and highly active next-generation libraries for CRISPR-mediated gene repression and activation. Elife 5, e19760. https://doi.org/10.7554/eLife.19760

Jost, M., Chen, Y., Gilbert, L.A., Horlbeck, M.A., Krenning, L., Menchon, G., Rai, A., Cho, M.Y., Stern, J.J., Prota, A.E., Kampmann, M., Akhmanova, A., Steinmetz, M.O., Tanenbaum, M.E., Weissman, J.S., 2017. Combined CRISPRi/a-Based Chemical Genetic Screens Reveal that Rigosertib Is a Microtubule-Destabilizing Agent. Mol Cell 68, 210-223 e6. https://doi.org/10.1016/j.molcel.2017.09.012

Kampmann, M., Bassik, M.C., Weissman, J.S., 2013. Integrated platform for genome-wide screening and construction of high-density genetic interaction maps in mammalian cells. Proc Natl Acad Sci U A 110, E2317-26. https://doi.org/10.1073/pnas.1307002110

Kitamura, H., Motohashi, H., 2018. NRF2 addiction in cancer cells. Cancer Sci 109, 900–911. https://doi.org/10.1111/cas.13537

Knutson, S.K., Warholic, N.M., Johnston, L.D., Klaus, C.R., Wigle, T.J., Iwanowicz, D., Littlefield, B.A., Porter-Scott, M., Smith, J.J., Moyer, M.P., Copeland, R.A., Pollock, R.M., Kuntz, K.W., Raimondi, A., Keilhack, H., 2014. Synergistic Anti-Tumor Activity of EZH2 Inhibitors and Glucocorticoid Receptor Agonists in Models of Germinal Center Non-Hodgkin Lymphomas. PLoS One 9, e111840. https://doi.org/10.1371/journal.pone.0111840

Kobayashi, H., Matsunaga, Y., Uchiyama, Y., Nagura, K., Komatsu, Y., 2013. Novel humanized anti-CD20 antibody BM-ca binds to a unique epitope and exerts stronger cellular activity than others. Cancer Med 2, 130–43. https://doi.org/10.1002/cam4.60

Lakhtakia, R., Burney, I., 2015. A Historical Tale of Two Lymphomas: Part II: Non-Hodgkin lymphoma. Sultan Qaboos Univ Med J 15, e317-21. https://doi.org/10.18295/squmj.2015.15.03.003

Lamar, Z.S., 2016. The Role of Glucocorticoids in the Treatment of Non- Hodgkin Lymphoma. Ann Hematol Oncol 3.

Law, L.W., 1956. Differences between cancers in terms of evolution of drug resistance. Cancer Res 16, 698–716.

Law, L.W., 1952. Effects of combinations of antileukemic agents on an acute lymphocytic leukemia of mice. Cancer Res 12, 871–8.

Lehar, J., Krueger, A.S., Avery, W., Heilbut, A.M., Johansen, L.M., Price, E.R., Rickles, R.J., Short, G.F., Staunton, J.E., Jin, X., Lee, M.S., Zimmermann, G.R., Borisy, A.A., 2009. Synergistic drug combinations tend to improve therapeutically relevant selectivity. Nat Biotechnol 27, 659–66. https://doi.org/10.1038/nbt.1549

Li, L., Wickham, T.J., Keegan, A.D., 2001. Efficient transduction of murine B lymphocytes and B lymphoma lines by modified adenoviral vectors: enhancement via targeting to FcR and heparan-containing proteins. Gene Ther 8, 938–45. https://doi.org/10.1038/sj.gt.3301487

Loewe, S., 1953. The problem of synergism and antagonism of combined drugs. Arzneimittelforschung 3, 285–90.

Lossos, I.S., Czerwinski, D.K., Alizadeh, A.A., Wechser, M.A., Tibshirani, R., Botstein, D., Levy, R., 2004. Prediction of survival in diffuse large-B-cell lymphoma based on the expression of six genes. N Engl J Med 350, 1828–37. https://doi.org/10.1056/NEJMoa032520

Ludeman, S.M., 1999. The chemistry of the metabolites of cyclophosphamide. Curr Pharm Des 5, 627–43.

Martin, M., 2011. Cutadapt removes adapter sequences from high-throughput sequencing reads. 2011 17, 3. https://doi.org/10.14806/ej.17.1.200

Michel, J.B., Yeh, P.J., Chait, R., Moellering, R.C., Kishony, R., 2008. Drug interactions modulate the potential for evolution of resistance. Proc Natl Acad Sci U A 105, 14918–23. https://doi.org/10.1073/pnas.0800944105

Moret, N., Clark, N.A., Hafner, M., Wang, Y., Lounkine, E., Medvedovic, M., Wang, J., Gray, N., Jenkins, J., Sorger, P.K., 2019. Cheminformatics Tools for Analyzing and Designing Optimized Small-Molecule Collections and Libraries. Cell Chem. Biol. 26, 765-777.e3. https://doi.org/10.1016/j.chembiol.2019.02.018

Murai, J., Tang, S.W., Leo, E., Baechler, S.A., Redon, C.E., Zhang, H., Al Abo, M., Rajapakse, V.N., Nakamura, E., Jenkins, L.M.M., Aladjem, M.I., Pommier, Y., 2018. SLFN11 Blocks Stressed Replication Forks Independently of ATR. Mol Cell 69, 371-384 e6. https://doi.org/10.1016/j.molcel.2018.01.012

Natkunam, Y., Farinha, P., Hsi, E.D., Hans, C.P., Tibshirani, R., Sehn, L.H., Connors, J.M., Gratzinger, D., Rosado, M., Zhao, S., Pohlman, B., Wongchaowart, N., Bast, M., Avigdor, A., Schiby, G., Nagler, A., Byrne, G.E., Levy, R., Gascoyne, R.D., Lossos, I.S., 2008. LMO2 protein expression predicts survival in patients with diffuse large B-cell lymphoma treated with anthracycline-based chemotherapy with and without rituximab. J Clin Oncol 26, 447–54. https://doi.org/10.1200/JCO.2007.13.0690

Neal, A.J., Hoskin, P.J., 2009. Clinical oncology : basic principles and practice, 4th ed. Hodder Arnold, London.

Odds, F.C., 2003. Synergy, antagonism, and what the chequerboard puts between them. J Antimicrob Chemother 52, 1. https://doi.org/10.1093/jac/dkg301

Paek, A.L., Liu, J.C., Loewer, A., Forrester, W.C., Lahav, G., 2016. Cell-to-Cell Variation in p53 Dynamics Leads to Fractional Killing. Cell 165, 631–642. https://doi.org/10.1016/j.cell.2016.03.025

Palmer, A.C., Sorger, P.K., 2017. Combination Cancer Therapy Can Confer Benefit via Patient-to-Patient Variability without Drug Additivity or Synergy. Cell 171, 1678-1691 e13. https://doi.org/10.1016/j.cell.2017.11.009

Pasqualucci, L., Trifonov, V., Fabbri, G., Ma, J., Rossi, D., Chiarenza, A., Wells, V.A., Grunn, A., Messina, M., Elliot, O., Chan, J., Bhagat, G., Chadburn, A., Gaidano, G., Mullighan, C.G., Rabadan, R., Dalla-Favera, R., 2011. Analysis of the coding genome of diffuse large B-cell lymphoma. Nat Genet 43, 830–7. https://doi.org/10.1038/ng.892

Penning, T.M., 2017. Aldo-Keto Reductase Regulation by the Nrf2 System: Implications for Stress Response, Chemotherapy Drug Resistance, and Carcinogenesis. Chem Res Toxicol 30, 162–176. https://doi.org/10.1021/acs.chemrestox.6b00319

Pritchard, J.R., Bruno, P.M., Gilbert, L.A., Capron, K.L., Lauffenburger, D.A., Hemann, M.T., 2013. Defining principles of combination drug mechanisms of action. Proc Natl Acad Sci U A 110, E170-9. https://doi.org/10.1073/pnas.1210419110

Rationalizing combination therapies, 2017. Rationalizing combination therapies. Nat Med 23, 1113. https://doi.org/10.1038/nm.4426

Reff, M.E., Carner, K., Chambers, K.S., Chinn, P.C., Leonard, J.E., Raab, R., Newman, R.A., Hanna, N., Anderson, D.R., 1994. Depletion of B cells in vivo by a chimeric mouse human monoclonal antibody to CD20. Blood 83, 435–45.

Roberts, A.M., Ward, C.C., Nomura, D.K., 2017. Activity-based protein profiling for mapping and pharmacologically interrogating proteome-wide ligandable hotspots. Curr Opin Biotechnol 43, 25–33. https://doi.org/10.1016/j.copbio.2016.08.003

Sanger, W.G., Eisen, J.D., 1976. Clastogenic effects of methylnitrosourea and ethylnitrosourea on chromosomes from human fibroblast cell lines. Mutat Res 34, 415–26.

Schnipper, L., 1986. Clinical implications of tumor-cell heterogeneity. N Engl J Med 314, 1423–31. https://doi.org/10.1056/NEJM198605293142206

Sebastian, E., Alcoceba, M., Martin-Garcia, D., Blanco, O., Sanchez-Barba, M., Balanzategui, A., Marin, L., Montes-Moreno, S., Gonzalez-Barca, E., Pardal, E., Jimenez, C., Garcia-Alvarez, M., Clot, G., Carracedo, A., Gutierrez, N.C., Sarasquete, M.E., Chillon, C., Corral, R., Prieto-Conde, M.I., Caballero, M.D., Salaverria, I., Garcia-Sanz, R., Gonzalez, M., 2016. High-resolution copy number analysis of paired normal-tumor samples from diffuse large B cell lymphoma. Ann Hematol 95, 253–62. https://doi.org/10.1007/s00277-015-2552-3

Shain, A.H., Pollack, J.R., 2013. The spectrum of SWI/SNF mutations, ubiquitous in human cancers. PLoS One 8, e55119. https://doi.org/10.1371/journal.pone.0055119

Shalem, O., Sanjana, N.E., Hartenian, E., Shi, X., Scott, D.A., Mikkelson, T., Heckl, D., Ebert, B.L., Root, D.E., Doench, J.G., Zhang, F., 2014. Genome-scale CRISPR-Cas9 knockout screening in human cells. Science 343, 84–87. https://doi.org/10.1126/science.1247005

Shibuya, T., Morimoto, K., 1993. A review of the genotoxicity of 1-ethyl-1-nitrosourea. Mutat Res 297, 3–38.

Skipper, H.E., Schabel, F.M., Wilcox, W.S., 1964. EXPERIMENTAL EVALUATION OF POTENTIAL ANTICANCER AGENTS. XIII. ON THE CRITERIA AND KINETICS ASSOCIATED WITH "CURABILITY" OF EXPERIMENTAL LEUKEMIA. Cancer Chemother. Rep. 35, 1–111.

Spencer, S.L., Gaudet, S., Albeck, J.G., Burke, J.M., Sorger, P.K., 2009. Non-genetic origins of cell-to-cell variability in TRAIL-induced apoptosis. Nature 459, 428–432. https://doi.org/10.1038/nature08012

Speth, P.A., van Hoesel, Q.G., Haanen, C., 1988. Clinical pharmacokinetics of doxorubicin. Clin Pharmacokinet 15, 15–31. https://doi.org/10.2165/00003088-198815010-00002

Sun, X., Vilar, S., Tatonetti, N.P., 2013. High-throughput methods for combinatorial drug discovery. Sci Transl Med 5, 205rv1. https://doi.org/10.1126/scitranslmed.3006667

Tanenbaum, M.E., Gilbert, L.A., Qi, L.S., Weissman, J.S., Vale, R.D., 2014. A protein-tagging system for signal amplification in gene expression and fluorescence imaging. Cell 159, 635–46. https://doi.org/10.1016/j.cell.2014.09.039

Thorn, C.F., Oshiro, C., Marsh, S., Hernandez-Boussard, T., McLeod, H., Klein, T.E., Altman, R.B., 2011. Doxorubicin pathways: pharmacodynamics and adverse effects. Pharmacogenet Genomics 21, 440–6. https://doi.org/10.1097/FPC.0b013e32833ffb56

Tran, L., Baars, J.W., Aarden, L., Beijnen, J.H., Huitema, A.D., 2010. Pharmacokinetics of rituximab in patients with CD20 positive B-cell malignancies. Hum Antibodies 19, 7–13. https://doi.org/10.3233/HAB-2010-0215

Wang, T., Wei, J.J., Sabatini, D.M., Lander, E.S., 2014. Genetic screens in human cells using the CRISPR-Cas9 system. Science 343, 80–4. https://doi.org/10.1126/science.1246981

Weiner, G.J., 2010. Rituximab: mechanism of action. Semin Hematol 47, 115–23. https://doi.org/10.1053/j.seminhematol.2010.01.011

Yeh, P.J., Hegreness, M.J., Aiden, A.P., Kishony, R., 2009. Drug interactions and the evolution of antibiotic resistance. Nat Rev Microbiol 7, 460–6. https://doi.org/10.1038/nrmicro2133

Zanotto-Filho, A., Masamsetti, V.P., Loranc, E., Tonapi, S.S., Gorthi, A., Bernard, X., Goncalves, R.M., Moreira, J.C., Chen, Y., Bishop, A.J., 2016. Alkylating Agent-Induced NRF2 Blocks Endoplasmic Reticulum Stress-Mediated Apoptosis via Control of Glutathione Pools and Protein Thiol Homeostasis. Mol Cancer Ther 15, 3000–3014. https://doi.org/10.1158/1535-7163.MCT-16-0271

Zoppoli, G., Regairaz, M., Leo, E., Reinhold, W.C., Varma, S., Ballestrero, A., Doroshow, J.H., Pommier, Y., 2012. Putative DNA/RNA helicase Schlafen-11 (SLFN11) sensitizes cancer cells to DNA-damaging agents. Proc Natl Acad Sci U A 109, 15030–5. https://doi.org/10.1073/pnas.1205943109

METHODS

Cell culture and chemotherapies

Diffuse Large B-Cell Lymphoma (DLBCL) cell lines were obtained from the American Type Culture Collection (ATCC) and the Dana Farber Cancer Institute. Identity of Pfeiffer cell line (ATCC® CRL-2632) was validated by Promega GenePrint 10 small tandem repeat (STR) profiling. All DLBCL cell lines were grown in RPMI-1640 with 25 mM HEPES and 2 mM L-alanine-L-glutamine (GlutaMAX) (Gibco 72400), supplemented to 4.5 g/L D-glucose, 10% (v/v) heat inactivated fetal bovine serum (FBS) (Gibco 16140071), and penicillin/streptomycin (P/S) at final concentrations of 100 U/mL and 100 µg/mL, respectively (Corning 30-002-CI). For CRISPRi screens, Pfeiffer cells were grown in RPMI-1640 (Gibco 72400) supplemented with 15% (v/v) FBS and P/S. K562 cells were grown in RPMI-1640 (ATCC 30-2001) with 10 mM HEPES, 4.5 g/L D-glucose, 2 mM L-glutamine, 1 mM sodium pyruvate, and supplemented with 10% (v/v) FBS and P/S. HEK293T cells were grown in Dulbecco's modified Eagle medium (Corning 10-013) with 4.5 g/L D-glucose, 4 mM L-glutamine, 1 mM sodium pyruvate, and supplemented with 10% (v/v) FBS and P/S. All cell lines were grown at 37 °C and 5% CO_2. Cells were tested for mycoplasma contamination using the MycoAlert mycoplasma detection kit (Lonza). When treating with rituximab alone or in combination, media was additionally supplemented with 5% (v/v) pooled complement human serum (HCS) (Innovative Research IPLA-CSER) to enable complement-mediated cytotoxicity. Cells were grown in vented tissue-culture treated polystyrene flasks. Cell density and viability was assessed during culture by a TC20 automated cell counter (Bio-Rad) with trypan blue; all cell densities reported here refer to the count of live cells with diameter between 8 and 24 µm. During culture before drug treatment experiments, DLBCL cells were maintained at the following densities: Pfeiffer between 3×10^5 and 15×10^5 cells/mL; SU-DHL-4 and SU-

DHL-6 between 2×10^5 and 10^6 cells/mL; with centrifugation and transfer to fresh media every 2 to 4 days.

Chemotherapies were obtained as follows: 4-hydroperoxy-cyclophosphamide (4HC) from Niomech (D-18864), doxorubicin, vincristine, and prednisolone from Selleck (S1208, S1241, and S1737), and rituximab from Dana Farber Cancer Institute. Single-use aliquots of 4HC were prepared in DMSO at -80°C, other chemotherapies were prepared in DMSO and stored at -20°C, and rituximab was prepared at 8 mg/mL in the clinical formulation plus 10% glycerol and stored at 4 °C. DMSO was obtained from Sigma (D2650) and puromycin from Gibco.

Measurement of drug-drug interactions

All drug interaction experiments were conducted in biological duplicates using two independent cultures of the same cell line. After being split from a common ancestor, cultures were propagated in parallel for at least one week before any experiment. Dose responses to single or multiple drugs were measured on DLBCL cells grown in sterile black polystyrene 384-well assay plates. Each well was inoculated with 30 μL of culture at density 10^5 cells/mL, and promptly afterwards concentration gradients of drugs were added to wells by D300 digital dispenser (Hewlett-Packard). All chemotherapies were dispensed as DMSO solutions, while rituximab was prepared at 2.5 mg/mL with 0.05% (v/v) Triton X-100, with a 90 s incubation after pipetting into the print cassette for liquid to be drawn into the print head. At the highest dispensed concentration of rituximab, this conferred a final Triton X-100 concentration of 3 parts-per-million, which we confirmed did not by itself inhibit the growth of DLBCL cells. Wells on plate edges were filled but not used for any measurements. The drug dispensing arrangement of each plate was spatially randomized (and re-organized during data analysis); thereby any spatial bias across a plate becomes random error rather than systematic error across dose responses. Whole control plates of untreated cultures demonstrated no detectable row bias or column bias. Each plate contained >40

untreated wells in randomized locations (not on edges) that served as no-inhibition controls. Assay plates were incubated at 37 °C with 5% CO_2, inside containers humidified by sterile wet gauze. After 72 h, plates were removed from incubation and cooled at room temperature for 30 min, before automated dispensing (BioTek EL406) of 30 µL of CellTiter-Glo (1:1 dilution in phosphate buffered saline (PBS)) into each well. Following a 10 min incubation at room temperature, each well's luminescence was measured in a plate reader (BioTek Synergy H1). At the time of the 384-well plates' initial seeding, 1.5 mL cultures in 6-well plates were prepared from the same cell suspension, with separate cultures including or excluding 5% HCS. At the time of drug addition to plates, one of each such culture was harvested, and cell density was counted (Bio-Rad TC20 using trypan blue), and 72 h later (at the time of CellTiter-Glo addition to 384-well plates) another such untreated 1.5mL culture was harvested and counted. From these density measurements we calculated the number of cell divisions occurring during the time of the assay, which was used during data analysis to determine Growth Rate (GR) metrics (Hafner et al., 2016). Specifically, we used GR = $\log_2$[(relative viability after treatment, according to CellTiter-Glo) × (cell number per µL of untreated control culture at t=72 h) / (cell number per µL of untreated control culture at t=0)] / $\log_2$[(cell number per µL of untreated control culture at t=72 h) / (cell number per µL of untreated control culture at t=0)] (Figure S1D). By this measure GR=1 indicates full, uninhibited growth, GR=0 indicates complete growth arrest, or that proliferation and death are in balance (final cell count = initial cell count), and GR<0 indicates net cytotoxicity (final cell count < initial cell count); note that we did not impose an asymptotic lower bound of -1 as described by Hafner et al (this would be computed as $2^{GR} - 1$). HCS slightly speeded the division rate of Pfeiffer in the absence of drugs (17% shorter doubling time), and slightly diminished Pfeiffer sensitivity to 4HC. Pairwise drug interactions (Figure 1) were measured over an 11×11 'checkerboard' of logarithmically-spaced drug concentrations (5 points per order of magnitude), with 5% HCS in media only in interactions with rituximab (for this reason 4HC is less potent in its isobologram with rituximab). The

concentration range for each drug was selected based on preliminary dose-ranging studies so as to span a range from no detectable effect on growth to 98% reduction in cell number relative to untreated control cells, which corresponds to growth arrest plus 90% cell killing. High-order drug interactions, including pairs (Figure 2), were measured over 14-point concentration gradients of one to five drugs, in all cases including 5% HCS so that drug sensitivity and drug-free cell division rate was consistent across conditions that would be compared in analysis. For these high-order interactions, each independent culture (biological replicate) was measured with cultures seeded into duplicate plates (plate-to-plate technical duplicates). Each of these four combinatorially complete drug response sets spanned two 384-well plates, which each contained a full set of single-drug gradients, and thus single-drug responses were in total measured in octuplicate. In the analysis, '100% luminescence' was defined on a per-plate basis by the interquartile mean of at least 50 drug-free wells within that plate (excluding edges). For isobologram analysis (Figure 1), the topology of drug response over the 11×11 checkerboards was smoothed by a nearest-neighbor median filter; this will apply no change to a monotonic response surface, and only smoothes data in cases of locally non-monotonic (that is, jagged) dose response. The absence of this filter changes no conclusions regarding interaction types but yields occasionally jagged isoboles. Fractional inhibitory concentrations (FICs) are calculated by comparing dose responses of drug combinations to dose responses of their constituent single drugs. Given a mixture of drugs at a dose that causes 50% killing, FIC_{50} is the sum of each drug's concentration in that mix as a fraction of the single-agent doses producing the same effect: $FIC_{50} = \sum \frac{IC50_{\text{drug in combination}}}{IC50_{\text{drug alone}}}$. FIC=1 indicates Loewe additivity.

Production of ClonTracer lentivirus

ClonTracer library was a gift from Frank Stegmeier (Addgene 67267). Lentiviral particles carrying ClonTracer were produced by calcium phosphate transfection of HEK293T cells (grown in DMEM with 10% FBS and 10 mM HEPES) with ClonTracer plasmid (10 μg per 10 cm dish) and lentiviral packaging

and VSV-G plasmids psPAX2 and pMD2.G (Cellecta CPCP-K2A; 10 µg of mix per 10 cm dish). Supernatants of transfected HEK293T cells were harvested at 48 h and again at 72 h post-transfection. Supernatants were pooled and clarified by centrifugation (500 ×g, 10 min). Lentiviral particles were concentrated from supernatant by mixing 3 parts supernatant with 1 part Lenti-X concentrator solution (ClonTech 631231), incubating overnight at 4 °C, centrifuging at 1500 ×g and 4 °C for 45 min, removing supernatant, and resuspending pellet at 1/100 original volume in PBS.

DNA Barcoding of cell lines

10^8 Pfeiffer cells in complete media were treated with 100 µg/mL N-ethyl-N-nitrosourea (ENU) for 4 h; this was previously determined to be the highest dose tolerable by Pfeiffer for this duration without conferring detectable cell death. Cells were washed twice and returned to drug-free media for 72 h to recover. 10^7 of these cells were infected with the ClonTracer lentiviral library by 'spinoculation'. In this protocol, five microcentrifuge tubes were prepared containing 2×10^6 cells in 1 mL complete media, with 8 µg/mL polybrene, and lentivirus at a volume yielding a multiplicity of infection (MOI) of 0.1 (per tube, this was 5 µL of 100× concentrate of lentivirus containing supernatant; see measurement of MOI below). Tubes were incubated for 10 min (37 °C, 5% CO_2), and centrifuged at 800 ×g and 37 °C for 60 min. The supernatant was removed, and each cell pellet was resuspended in 4 mL complete media (5×10^5 cells/mL) and transferred to one well of a 6-well plate for continued growth (incubation at 37 °C, 5% CO_2). Volume of lentivirus to produce this MOI had been previously determined by test infections of Pfeiffer with different volumes of lentiviral solution, after which the fraction of infected Pfeiffer cells were counted by flow cytometric analysis of the red fluorescent protein encoded by the ClonTracer cassette (BD LSRII, ex:488nm, em:575/26nm), having first gated out dead cells (Violet Viability kit, Thermo Fisher Scientific L34958, ex:405nm, em:450/50nm) (note, red fluorescence was not readily detectable until 2 days post-infection). From the measured fraction of fluorescent cells, MOI was

calculated assuming a Poisson distribution of infection events. Cells were expanded in complete media for 3 days before applying selection for infected cells (which carry a puromycin resistance gene in the ClonTracer cassette): 3 days in 0.25 μg/mL, 3 days in 0.5 μg/mL, and then 2 days in 1 μg/mL puromycin. At this time flow cytometry could not detect a significant population of non-fluorescent cells. Barcoded Pfeiffer cells were grown without puromycin for an additional 4 days before selection experiments in R-CHOP.

Selection for drug resistant clones

From a well-mixed suspension of barcoded Pfeiffer cells, 10^8 cells were harvested and frozen for measurement of pre-treatment DNA barcode frequencies by sequencing. From the same suspension of cells and at the same time, 15 replicate cultures were prepared in 75 cm^2 flasks with 25 mL of complete media containing 5×10^5 cells/mL of barcoded Pfeiffer cells. The total count of 12.5×10^6 cells per flask is calculated to contain 99.999% of the 10^6 unique clones assuming equal initial abundance and random assortment into flasks. Because rituximab displayed an 'inoculum effect' with limited cytotoxicity at high cell density, 3 cultures for rituximab treatment were prepared at lower density and higher volume: 60 mL of barcoded Pfeiffer at 1×10^5 cells/mL in 150 cm^2 flasks, in media supplemented with 5% HCS. The total count of 6×10^6 cells in each rituximab-treated flask is calculated to contain 99.7% of the 10^6 clones. For each drug, and DMSO control, three replicate flasks were treated for 72 h at the following concentrations: 4 μM 4HC; 50 nM doxorubicin; 5.6 nM vincristine; 16 μg/mL rituximab; 0.04% (i.e., 0.0004) (v/v) DMSO (the highest DMSO concentration delivered with any drug). These drug concentrations were chosen on the basis of preliminary dose-finding experiments that identified them to be the highest concentration, in a series of 2-fold concentration steps, from which any surviving cells repopulated the culture within 2 weeks of recovery following the 72 h drug treatment. Following treatment, cultures were washed twice and resuspended in drug-free media. During recovery, culture

volumes were adjusted to maintain cell density within the recommended range (3-15×10^5 cells/mL). No cells were disposed of except from the DMSO control flasks, which suffered no inhibition but were maintained for a 'recovery' time to match drug-treated flasks. Following recovery to a population size twice the initial inoculum, the recovered cultures were exposed to repeat treatments (each flask treated by the same drug as before), and recovery. Following the second recovery, cultures were centrifuged and cell pellets harvested for barcode sequencing. Prednisolone treatments were designed differently because it was not cytotoxic to cultured Pfeiffer cells (nor any of six other DLBCL cell lines) in concentrations up to 50 μM. Therefore, triplicate Pfeiffer cultures (25 mL in 75 cm^2 flasks) were maintained in 20 μM prednisolone for 20 days, with cell density maintained between 3-15×10^5 cells/mL and with fresh prednisolone administered with media changes every 72 to 96 h (Figure S3A). This treatment duration was estimated to produce ≈20-fold enrichment of clones fully resistant to the mild inhibitory effect of prednisolone (≈13 divisions in 20 days ⇒ enrichment from resisting 20% growth inhibition = $(1 / 0.8)^{13}$ = 18-fold).

Barcode amplification and sequencing

To avoid contamination of pre-amplification materials with amplified DNA barcodes (which are approximately a billion-fold more concentrated), all materials, processes and equipment used prior to PCR amplification of ClonTracer barcodes were physically and temporally quarantined from all materials, processes and equipment used following PCR (distant benches and equipment, never both used on the same day). Genomic DNA (gDNA) was extracted from frozen cell pellets with DNeasy Blood and Tissue extraction kits (Qiagen 69504), using the spin-column protocol including RNase A incubation. Four spin columns were used per sample of 10-15×10^6 cells; whereas the pre-treatment sample was a larger population of 3×10^7 cells applied to 8 spin columns. DNA concentration was measured by SYBR green fluorescence with a λ dsDNA calibration curve (readings on BioTek Synergy

H1). ClonTracer DNA barcodes consist of a repeating 'Strong (G or C) - Weak (A or T)' pattern with no detectable PCR amplification bias so that barcode counts measured by deep sequencing are proportional to clone abundance (Bhang et al., 2015). Barcodes were amplified from 20 μg of gDNA per sample, representing 3 million diploid genomes as template, with Q5 polymerase (New England Biolabs M0492). This was accomplished with parallel 50 μL reactions with 2 μg of template each. The pre-treatment sample was amplified from 20μg of DNA, representing 6 million genomes. Primer sequences were as described previously (see Supplemental Table 2 of Bhang et al. (2015)). Reaction success and yield was verified by agarose gel electrophoresis. PCR products of all treatment conditions were pooled and size selected (133 bp) by excision from an agarose gel (using SYBR-safe stain and blue LED illumination) with purification by QIAquick Gel Extraction Kit (Qiagen 28704). PCR product from pre-treatment cell sample was processed separately rather than pooled with others. PCR products were sequenced on Illumina HiSeq 2500 in high-output single read mode, with custom read (CCGAGATACTGACTGCAGTCTGAGTCTGACAG) and index (AGCAGAGCTACGCACTCTATGCTAG) primers. A 30% PhiX spike-in provided necessary sequence diversity. FASTQ files were analyzed by the clonTracer_analyze v1.0 script which is available with the ClonTracer system (see www.addgene.org, cat. #67267). This script conducts the Barcode-composition analysis described by Bhang et al. (2015), which identifies high-quality reads that conform to the expected barcode pattern (30nt of alternating weak (A/T) then strong (G/C)), and merges barcode sets that contain one high abundance barcode and sequence-adjacent barcodes (hamming distance 1 or 2) at much lower abundance indicating that they are sequencing errors of the high-abundance barcode. For each drug treated sample, 6-8×10^6 barcode reads were obtained, and from the pre-treatment sample 1.6×10^8 barcode reads were obtained; the latter being sequenced at greater depth.

Analysis of barcode enrichment

Barcode counts in the pre-treatment sample were assigned a lower bound of the 5% quantile of counts in this sample (34 counts); this prevents barcodes that were rare or undetected in the pre-treatment sample from scoring as highly enriched in a drug treatment while having, for example, only 2 reads. Absolute barcode counts in pre- and post-treatment samples were then converted to the fraction of all counts for that sample. Each barcode's enrichment in a given drug treatment was calculated as post-treatment frequency divided by pre-treatment frequency. The biological triplicates of each treatment were merged to a single score by calculating the geometric mean enrichment. Each repeat was assigned a minimum enrichment of 1 when calculating geometric mean, to prevent severely penalizing barcodes that were not detected in one of three repeats; this is motivated by the statistical possibility that a barcode may be absent from any one flask's inoculum. A small fraction of barcodes exhibited geometric mean enrichment >1 in DMSO-treated cultures (1% of barcodes were enriched ≥ 10-fold), and therefore to normalize for these differences in fitness that are unrelated to drug sensitivity, we divided each barcode's enrichment scores in drug treatments by its enrichment in DMSO only when DMSO-enrichment was greater than 1 (enrichment scores in a drug treatment were not increased by having DMSO enrichment score less than 1).

Lentivirus production for CRISPR reagents

HEK293T cells were transfected with the lentiviral plasmid of interest (as mentioned in relevant sections below), psPAX2 (Addgene #12260) and pCMV-VSV-G (Addgene #8454) in a 2:2:1 molar ratio using lipofectamine 3000 (Invitrogen) according to the manufacturer's instructions. The growth medium was replaced 6 h post-transfection and was then harvested at 28 h and 52 h post-transfection. The two harvested growth medium fractions were pooled, centrifuged at 1,000 ×g for 10 min, and filtered through a 0.45 μm low-protein binding membrane. Lentivirus containing supernatants were stored at -80

°C. If needed, lentivirus titers were increased by adding ViralBoost reagent (Alstem) to the cell culture medium and lentivirus supernatants were concentrated using a lentivirus precipitation solution (Alstem).

Generation of Cas9-expressing cell lines

To generate the Pfeiffer cell line stably expressing dCas9-KRAB (Pfeiffer CRISPRi), Pfeiffer cells (ATCC CRL-2632) were transduced with lentiviral particles produced using vector pMH0001 (Addgene #85969; expresses dCas9-BFP-KRAB from a spleen focus forming virus (SFFV) promoter with an upstream ubiquitous chromatin opening element) in the presence of 8 µg/mL polybrene. A pure polyclonal population of dCas9-KRAB expressing cells was generated by 3 rounds of fluorescence activated cell sorting (FACS) gated on the top half of BFP positive cells (BD FACS Aria II).

To generate the K562 cell line stably co-expressing dCas9 fused to the SunTag, and a SunTag-binding antibody fused to the VP64 transcriptional activator (K562 CRISPRa), K562 cells (ATCC CCL-243) were first transduced with lentiviral particles produced using vector pHRdSV40-dCas9-10xGCN4_v4-P2A-BFP (Addgene #60903; expresses dCas9 tagged with 10 copies of the GCN4 peptide v4 and BFP) in the presence of 8 µg/mL polybrene. After selection of BFP positive cells using one round of FACS (BD FACS Aria II), cells were transduced with lentiviral particles produced using vector pHRdSV40-scFv-GCN4-sfGFP-VP64-GB1-NLS (Addgene #60904; expresses a single chain variable fragment (scFv) that binds to the GCN4 peptide from the SunTag system, in fusion with superfolder green fluorescent protein (sfGFP) and VP64) in the presence of 8 µg/mL polybrene. Single cells with high GFP levels (top 25% of GFP positive cells) and high BFP levels (top 50% of BFP positive cells) were isolated by FACS and grown in single wells of a 96-well plate. Monoclonal cell lines were expanded and tested for their ability to increase the expression of target control genes (see section below). A single clone exhibiting robust growth and robust overexpression of target genes was selected as cell line K562 CRISPRa.

Evaluation of CRISPRi/a cell lines using sgRNAs targeting individual genes

Pairs of complementary synthetic oligonucleotides (Integrated DNA Technologies) forming sgRNA protospacers flanked by BstXI and BlpI restriction sites were annealed and ligated into BstXI/BlpI double digested plasmid pU6-sgRNA EF1Alpha-puro-T2A-BFP (Addgene #60955). Oligonucleotides used to build sgRNA targeting individual genes are listed in Table S1. The sequence of all sgRNA expression vectors was confirmed by Sanger sequencing and lentiviral particles were produced using these vectors as described above (see "lentivirus production"). Pfeiffer CRISPRi and K562 CRISPRa cells were infected with individual sgRNA expression vectors by addition of lentivirus supernatant to the culture medium in the presence of 8 µg/mL polybrene. Transduced cells were selected using puromycin (0.8 µg/mL for Pfeiffer and 2 µg/mL for K562) starting 48 h post-transduction and over the course of 7 days with daily addition of the antibiotic. After 24 h growth in puromycin-free medium, 1×10^5 cells were harvested and total RNA was extracted using the RNeasy Plus Mini kit (Qiagen). cDNA was synthesized from 0.1 µg total RNA using Superscript IV reverse transcriptase (Invitrogen) and oligo$(dT)_{20}$ primers (Invitrogen), following the manufacturer's instructions. Reactions were diluted 4-fold with H_2O and qPCR was performed in 10 µL reaction volume in 96-well plates using PowerUp SYBR Green PCR Master mix (Thermo Fisher Scientific), 2 µL diluted cDNA preparation, and 0.4 µM of primers. All qPCR primers are listed in Table S1. To calculate changes in expression level of target genes, all gene specific Ct values were first normalized to the Ct value of a reference gene (GAPDH) to find a ΔCt value. Log_2 fold changes in expression were then determined by the difference between the ΔCt value of targeting sgRNAs and that of a non-targeting negative control sgRNA (ΔΔCt).

CRISPRi/a screens

Genome-wide libraries of sgRNAs from Addgene (hCRISPRi_v2: #83969 and #83970; hCRISPRa_v2: #83978 and #83979; a gift from Jonathan Weissman (Horlbeck et al., 2016)) were amplified in MegaX

DH10B T1R cells (Invitrogen). These two libraries are provided as two sub-libraries each containing about 100,000 individual plasmids (5 sgRNAs per gene). Sub-libraries (100 ng) were electroporated into MegaX DH10B T1R cells according to the manufacturer's instructions and the resulting transformed cells were plated on 10× 150 mm LB/Ampicillin (100 µg/mL) Petri dishes. After 17 h at 30 °C, cells were scraped off the plates, washed with LB, and plasmid DNA was prepared from the cell pellet using the Plasmid Plus Maxi kit (Qiagen). Coverage for each sub-library was determined by serial dilution and colony counting, and was at least 5,000× for each sub-library. Lentiviral supernatant was prepared using an equimolar ratio of each sub-library plasmid for both the hCRISPRi_v2 and the hCRISPRa_v2 sgRNA libraries as described above ("lentivirus production") and was stored at -80 °C. The multiplicity of infection (MOI) of both preparations was determined by titration onto the target cell line and quantification of the percentage of BFP positive cells 2-3 days post-transduction by flow cytometry (BD Biosciences LSR II).

For CRISPRi screens, Pfeiffer CRISPRi cells (2.5×10^8) were transduced with the hCRISPRi_v2 library lentivirus at an MOI of 0.4 in 250 mL culture medium + 8 µg/mL polybrene in 3× 225 cm^2 cell culture flasks (Costar). 24 h post-transduction, cells were harvested and resuspended in 400 mL fresh medium in 4× 225 cm^2 cell culture flasks. Starting 48h post-transduction, the culture medium was exchanged daily and cells were maintained at 0.8×10^6/mL in puromycin (0.8 µg/mL) in 400-500 mL. After 5 days in puromycin, the proportion of BFP positive cells determined by flow cytometry increased from 37% to 90% of the fraction of viable cells. After recovery for 1 day in puromycin-free medium, the library cells were ready for initiation of parallel drug selections. First, a T0 sample of 6×10^7 cells was harvested and stored at -80 °C. Each screen was initiated using 6×10^7 cells at 0.4×10^6/mL in 2× 225 cm^2 cell culture flasks. Vincristine (O), 4-hydroperoxy-cyclophosphamide (C), and Doxorubicin (H) were added from 500× stocks in DMSO. A DMSO-only screen was used as an untreated control screen. Rituximab (R) was added from a 2 mg/mL stock in PBS and 5% (v/v) HCS was added to the growth medium. A screen

with matching treatment of 5% (v/v) HCS was used as an untreated control screen for rituximab. For the duration of the screen, cells were maintained in 2× 225 cm^2 cell culture flasks at a minimum concentration of 0.4×10^6/mL in 150 mL (minimum coverage of 300 cells per sgRNA) by exchanging the medium to fresh medium every 2 days. For drug treatment, cells were treated with pulses of drug for 3 days followed by exchange of the growth medium. O (5.0 nM final concentration) was added on day 0, day 7 and day 11; C (3.3 μM) was added on day 0 and day 3; H (27 nM) was added on day 0 and day 7; R (4 μg/mL and 5% HCS) was added on day 0, day 5 and day 10. During the course of the screen, cell count and viability were measured using a TC20 automated cell counter (Bio-Rad) using trypan blue. The vincristine CRISPRi screen underwent 7.60 fewer population doublings than the DMSO control screen; the 4-hydroperoxy-cyclophosphamide screen underwent 9.34 fewer doublings; and the doxorubicin screen underwent 7.41 fewer doublings. The rituximab CRISPRi screen underwent 7.53 fewer population doublings than the 5% HCS control screen. At day 14, 8×10^7 cells were harvested from each screen by centrifugation, washed twice with PBS and gDNA was extracted using the QIAamp DNA Blood Maxi Kit (Qiagen) according to the manufacturer's instruction, except that the elution was performed using 10 mM Tris·HCl pH 8.5. Typical yields from 8×10^7 cells ranged from 500-650 μg gDNA.

For CRISPRa screens, K562 CRISPRa cells (3×10^8) were transduced with the hCRISPRa_v2 library lentivirus at an MOI of 0.25 in 300 mL culture medium + 8 μg/mL polybrene in 3× 225 cm^2 cell culture flasks (Costar). 24 h post-transduction, cells were harvested and resuspended in 450 mL fresh medium in 4× 225 cm^2 cell culture flasks. Starting 48h post-transduction, the culture medium was exchanged daily and cells were maintained at 0.8×10^6/mL in puromycin (1.5-1.75 μg/mL) in 400-500 mL. After 5 days in puromycin, the proportion of BFP positive cells determined by flow cytometry increased from 26% to 96% of the fraction of viable cells. After recovery for 1 day in puromycin-free medium, the library cells were ready for initiation of parallel drug selections. First, a T0 sample of 8×10^7 cells was

harvested and stored at -80 °C. Each screen was initiated using 6×10^7 cells at 0.4×10^6/mL in 2× 225 cm^2 cell culture flasks. Vincristine (O), 4-hydroperoxy-cyclophosphamide (C), and Doxorubicin (H) were added from 500× stocks in DMSO. A DMSO-only screen was used as an untreated control screen. For the duration of the screen, cells were maintained in 2× 225 cm^2 cell culture flasks at a minimum concentration of 0.4×10^6/mL in 150 mL (minimum coverage of 300 cells per sgRNA) by exchanging the medium to fresh medium every 2 days. For drug treatment, cells were treated with pulses of drug for 3 days followed by exchange of the growth medium. O (35.0 nM final concentration) was added on day 0 and day 8; C (7.5 μM) was added on day 0 and day 8; H (27 nM) was added on day 0 and day 8. During the course of the screen, cell count and viability were measured using a TC20 automated cell counter using trypan blue. The vincristine CRISPRa screen underwent 8.80 fewer population doublings than the DMSO control screen; the 4-hydroperoxy-cyclophosphamide screen underwent 10.52 fewer doublings; and the doxorubicin screen underwent 9.87 fewer doublings. At day 15, 8×10^7 cells were harvested from each screen by centrifugation, washed twice with PBS and gDNA was extracted using the QIAamp DNA Blood Maxi Kit according to the manufacturer's instruction, except that the elution was performed using 10 mM Tris·HCl pH 8.5. Typical yields from 8×10^7 cells ranged from 500-680 μg gDNA.

sgRNA barcode sequences were amplified by PCR using the extracted gDNA from either CRISPRi or CRISPRa screens as template and Phusion (NEB M0530) as polymerase. An equimolar mix of primers with stagger regions of different length (CC_LSP_025 to CC_LSP_032) was used as forward primer (to maintain sequence diversity in the common linker region for high-throughput sequencing purposes) and barcoded index primers (CC_LSP_033 to CC_LSP_040) were used as reverse primers. Reactions were composed of 1× HF buffer, 0.2 mM dNTPs, 0.4 μM forward primer mix, 0.4 μM indexed reverse primer, 0.5 μL Phusion, 1.5 mM $MgCl_2$, and 5 μg gDNA in a volume of 50 μL. After initial melting at 98 °C for 30 s, the reactions were subjected to 24 cycles of heating at 98 °C for 30 s, annealing at 62 °C for 30 s and extension at 72 °C for 30 s, and were followed by a final extension step at 72 °C for 5 min.

After verification of the PCR reaction success by agarose gel electrophoresis using SYBR safe stain (Thermo Fisher Scientific) on a single 50 µL reaction, 50% of the extracted gDNA for each screen (gDNA from 4×10^7 cells, corresponding to a coverage of 200×) was used as template in PCR reactions (typically 50-70 reactions per screen). After pooling all reactions from each single screen, the amplified sgRNA barcode PCR product (~240-250 bp) was purified by agarose gel electrophoresis using the QIAquick gel extraction kit (Qiagen). The concentration of individual libraries was quantified by fluorescence using the Qubit dsDNA high sensitivity assay kit (Thermo Fisher Scientific). Individual indexed libraries were mixed in equimolar ratio and were further purified using a QIAquick PCR purification kit (Qiagen). After determining accurate concentrations by quantitative PCR using the NEBnext library quant kit for Illumina (NEB), pooled libraries were sequenced on an Illumina HiSeq 2500 platform using a 50 bp single read on a high output standard v4 flow cell with a 15-20% PhiX spike-in. A total of 51-72 million reads were obtained for each indexed screen (minimum coverage of 250×).

The fastq sequencing files were analyzed using a Python-based ScreenProcessing pipeline previously reported by Horlbeck et al. (2016) (https://github.com/mhorlbeck/ScreenProcessing) with the following modification introduced due to the use of a mix of forward primers with a staggered region of different length. All reads were first processed using Cutadapt (Martin, 2011) to remove the linker sequence in front of the sgRNA barcode in each read (CTTGGAGAACCACCTTGTTG). To count the abundance of each sgRNA barcode in every sample, trimmed sequences were aligned to the library of protospacers present in the hCRISPRi_v2 or hCRISPRa_v2. Typically, 83-87% of the number of raw reads were aligned to the library of protospacers. The count files were next used to generate negative control genes, and calculate enrichment phenotypes and Mann-Whitney p-values as previously described (Gilbert et al., 2014; Horlbeck et al., 2016). To estimate technical noise in the screen, simulated negative control genes (the same number as that of real genes) were generated by randomly grouping 10 sgRNAs from the pool

of ~4,000 non-targeting control sgRNAs present in the libraries. The phenotypic effect of each sgRNA was quantified by the rho phenotype metric (Kampmann et al., 2013) which calculates the log2 fold change in abundance of an sgRNA between the treated and vehicle control samples, subtracting the equivalent median value for all 4,000 non-targeting sgRNAs, and dividing by the number of population doubling differences between the treated and vehicle control populations. Similarly, untreated growth phenotypes ('gamma' phenotypes) can be calculated by a comparison of vehicle control and T0 samples; and 'tau' phenotypes can be calculated by a comparison of treated and T0 samples (Gilbert et al., 2014; Kampmann et al., 2013). For each gene (and simulated control gene), which is targeted by 10 sgRNAs, two metrics were calculated: (i) the mean of the strongest 5 rho phenotypes by absolute value, and (ii) the p-value of all 10 rho phenotypes compared to the 4,000 non-targeting control sgRNAs (Mann-Whitney test). For genes with multiple independent transcription start sites (TSSs) targeted by the sgRNA libraries, the two metrics were calculated independently for each TSS and the TSS with the lowest Mann-Whitney p-value was chosen for further analysis. sgRNAs were required to have a minimum of 25 counts in at least one of the two conditions tested to be included in the analysis. To deal with the noise associated with potential low count numbers, a pseudocount of 10 was added to all counts. Genes that had less than 8 sgRNA rho phenotypes were not included for further analysis. Read counts and phenotype scores for individual sgRNAs are available in the Supplemental Data. Gene-level phenotype scores and p-values are available in the Supplemental Data.

CRISPRi cyclophosphamide hypersensitivity screen

The additional CRISPRi cyclophosphamide screen (Figure S5B) for identification of hypersensitive hits was performed and analyzed as described above with the following key modifications. Pfeiffer CRISPRi cells (2×10^8) were transduced with the top 5 half library of hCRISPRi_v2 (Addgene #83969, i.e. 5 sgRNAs per gene) at an MOI of 0.3 in 200 mL culture medium + 8 µg/mL polybrene in 2× 225 cm^2 cell

culture flasks. 24 h post-transduction, cells were harvested and resuspended in 300 mL fresh medium in 3× 225 cm^2 cell culture flasks. Starting 48h post-transduction, the culture medium was exchanged daily and cells were maintained at 0.8×10^6/mL in puromycin (0.6 µg/mL) in 300-400 mL. After 3 days in puromycin, cells were recovered for 1 day in puromycin-free medium. A T0 sample of 5×10^7 cells was harvested and stored at -80 °C. The CRISPRi screen was initiated using 2.5×10^7 cells at 0.4×10^6/mL in 1× 225 cm^2 cell culture flask. For the duration of the screen, cells were maintained in 1× 225 cm^2 cell culture flask at a minimum concentration of 0.4×10^6/mL in 62.5 mL (minimum coverage of 250 cells per sgRNA) by exchanging the medium to fresh medium every 2 days. 4-hydroperoxy-cyclophosphamide (2.5 µM final concentration) was added on day 0 and day 8. The cyclophosphamide CRISPRi screen underwent 4.38 fewer population doublings than the DMSO control screen. At day 15, gDNA was extracted from 5×10^7 cells from each screen and half of that was used as template in PCR reactions (coverage of 250×). A total of 31-34 million reads were obtained for each indexed sample and 81-82% of those reads were aligned to the reference library of protospacers. Negative control genes were generated by randomly grouping 5 sgRNAs from the pool of ~2,000 non-targeting control sgRNAs present in the half-library. For each gene (and simulated control gene), which is targeted by 5 sgRNAs, two metrics were calculated: (i) the mean of the strongest 3 rho phenotypes by absolute value, and (ii) the p-value of all 5 rho phenotypes compared to the 2,000 non-targeting control sgRNAs (Mann-Whitney test). Low count numbers were dealt with by adding a pseudocount of 1 to all zero counts. Gene ontology analysis was performed on the full output list of genes ranked by hypersensitivity score using GOrilla (Eden et al., 2009). The reported p-value is the enrichment p-value computed according to the GOrilla algorithm. The 'FDR q-value' represents the correction of the p-value for multiple testing hypothesis.

Cross-resistance analysis of CRISPR screens

For each gene, a single aggregate resistance score was calculated by multiplying the two metrics determined in the screen processing pipeline (resistance score = $-\log_{10}$(Mann-Whitney p-value)×mean of the strongest 5 rho phenotypes). Genes required 8 or more observed sgRNA rho phenotype scores in a specific screen for inclusion in the analysis. In order to account more accurately for the technical noise in the screen, 10 random sets of ≈19,000 simulated control genes were generated (matching the number of actual gene targets). A resistance score was then calculated for each simulated control gene in all 10 sets for all the drugs tested (4 for CRISPRi and 3 for CRISPRa). Genes that have a resistance score above a specific cutoff in at least 2 conditions tested are defined as 'cross-resistant'. The cutoff for cross-resistance analysis was determined by systematically quantifying the number of simulated control genes that would score as cross-resistant over the full range of resistance score cutoffs (in 0.01 increments). We selected a cutoff that scored on average over the 10 sets of control genes a single (or less than one) double resistant negative control simulated gene over all possible two drug combinations. Cross-hypersensitivity analyses were performed in an analogous way (the hypersensitivity score was calculated in the same way as the resistance score).

Quantifying cross-resistance in clone tracing and CRISPR screens

Strength of cross-resistance for different sets of drugs was quantified as a weighted sum of the maximum and minimum cross-resistance scenarios. Given rates of single-drug resistance 10^{-A} and 10^{-B} to drugs *a* and *b*, the theoretical minimum rate of cross-resistance is 10^{-A-B} (this scenario is indicated by cross-resistance parameter $\xi = 0$), and the theoretical maximum rate of cross-resistance is min(10^{-A} or 10^{-B}) (this scenario is indicated by cross-resistance parameter $\xi = 1$). Given an observed frequency of multi-drug resistance (MDR), cross-resistance ξ is computed as the solution to the equation: MDR frequency = $\xi \times$ minimum(10^{-A} or 10^{-B}) + $(1 - \xi) \times 10^{-A-B}$. This solution is $\xi = (10^{-A-B} - \text{MDR}) / (10^{-A-B} - \text{minimum}(10^{-A} \text{ or } 10^{-B}))$.